AD-A047 005 DAVID W TAYLOR NAVAL SHIP RESEARCH AND DEVELOPMENT CE--ETC F/G 13/10
COMPARISON OF EXPERIMENTAL DATA WITH ANALYTICAL PREDICTIONS (IN--ETC(U)
OCT 77 B L FISHER, E S BAKER

UNCLASSIFIED SPD-751-01 NL

1 OF 1
ADA047005

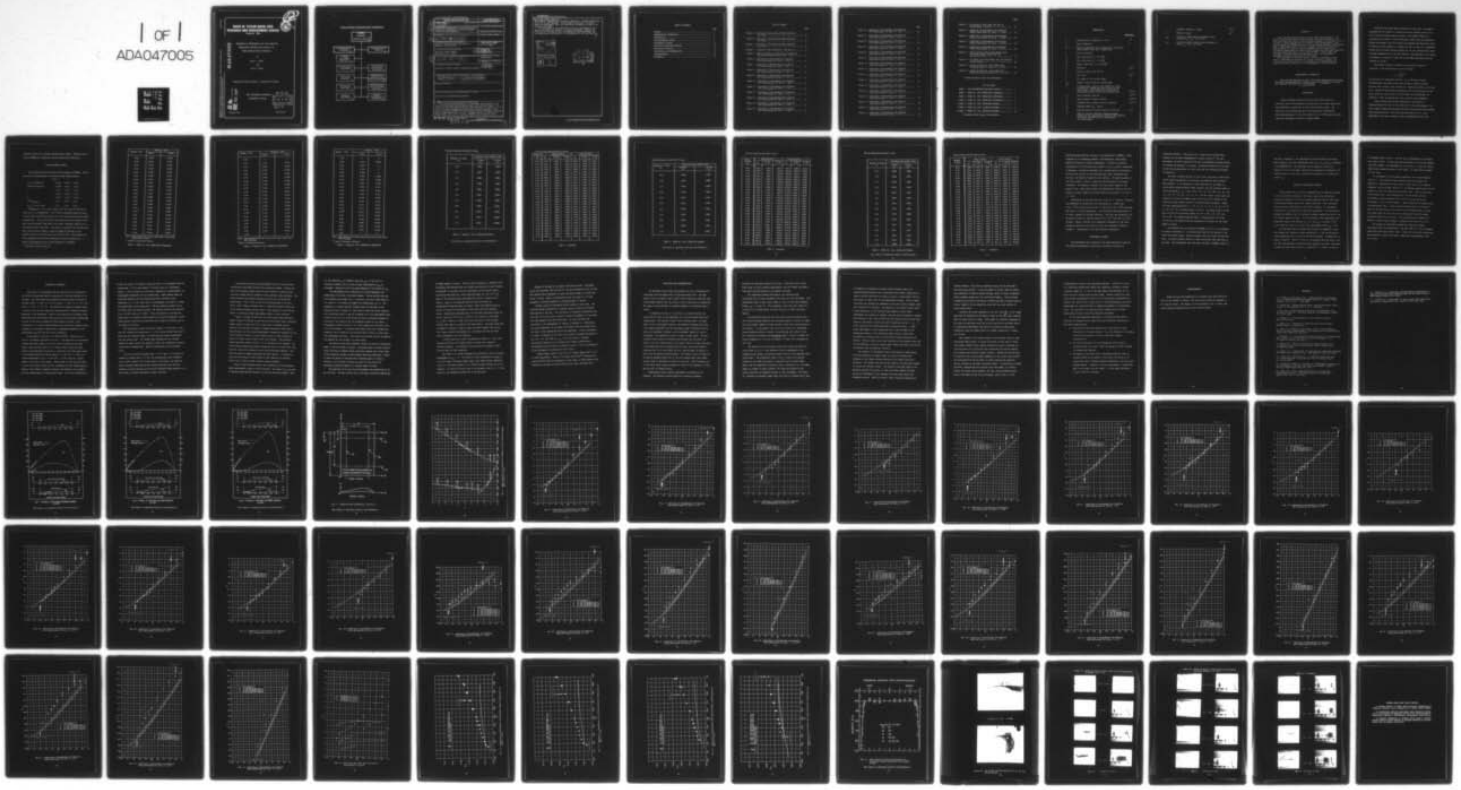

END
DATE FILMED
1-78
DDC

SPD-751-01

COMPARISON OF EXPERIMENTAL DATA WITH ANALYTICAL PREDICTIONS (INCLUDING WALL EFFECT) FOR THREE SUPERCAVITATING HYDROFOILS

DAVID W. TAYLOR NAVAL SHIP RESEARCH AND DEVELOPMENT CENTER

Bethesda, Md. 20084

AD A047005

COMPARISON OF EXPERIMENTAL DATA WITH ANALYTICAL PREDICTIONS (INCLUDING WALL EFFECT) FOR THREE SUPERCAVITATING HYDROFOILS

by

Barry L. Fisher

and

Elwyn S. Baker

APPROVED FOR PUBLIC RELEASE: DISTRIBUTION UNLIMITED

AD No.
DDC FILE COPY

SHIP PERFORMANCE DEPARTMENT

DEPARTMENTAL REPORT

DDC
RECEIVED
DEC 5 1977
D

October 1977

SPD-751-01

MAJOR DTNSRDC ORGANIZATIONAL COMPONENTS

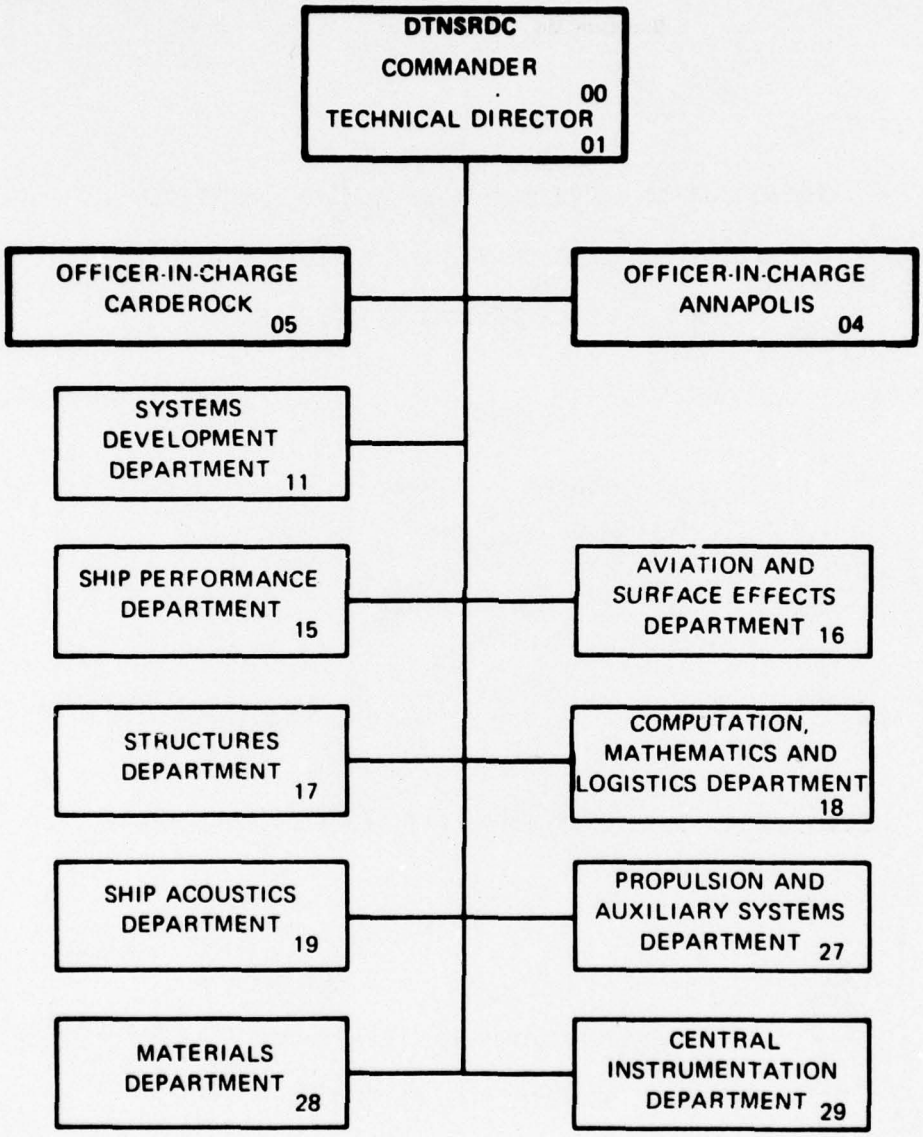

SECURITY CLASSIFICATION OF THIS PAGE (When Data Entered)

REPORT DOCUMENTATION PAGE

READ INSTRUCTIONS BEFORE COMPLETING FORM

(14) 1. REPORT NUMBER: SPD-751-01 ✓

2. GOVT ACCESSION NO.

3. RECIPIENT'S CATALOG NUMBER

(6) 4. TITLE (and Subtitle): COMPARISON OF EXPERIMENTAL DATA WITH ANALYTICAL PREDICTIONS (INCLUDING WALL EFFECT) FOR THREE SUPERCAVITATING HYDROFOILS.

5. TYPE OF REPORT & PERIOD COVERED

6. PERFORMING ORG. REPORT NUMBER

(10) 7. AUTHOR(s): Barry L. Fisher [redacted] Elwyn S. Baker

8. CONTRACT OR GRANT NUMBER(s)

9. PERFORMING ORGANIZATION NAME AND ADDRESS
David W. Taylor Naval Ship R&D Center ✓
Bethesda, Maryland 20084

10. PROGRAM ELEMENT, PROJECT, TASK AREA & WORK UNIT NUMBERS
Task Area ZF43321001
4 62543N

11. CONTROLLING OFFICE NAME AND ADDRESS
Naval Sea Systems Command
Washington, D.C. 20350

(11) 12. REPORT DATE: October 1977

13. NUMBER OF PAGES: 77

(9) 14. MONITORING AGENCY NAME & ADDRESS (if different from Controlling Office): Departmental rept.,

15. SECURITY CLASS. (of this report): UNCLASSIFIED

15a. DECLASSIFICATION/DOWNGRADING SCHEDULE

16. DISTRIBUTION STATEMENT (of this Report)

(12) 80p.

APPROVED FOR PUBLIC RELEASE: DISTRIBUTION UNLIMITED

17. DISTRIBUTION STATEMENT (of the abstract entered in Block 20, if different from Report)

(16) F43421 (17) ZF4342101

18. SUPPLEMENTARY NOTES

19. KEY WORDS (Continue on reverse side if necessary and identify by block number)

Wall Effect, Supercavitating, Hydrofoil

20. ABSTRACT (Continue on reverse side if necessary and identify by block number)

Three supercavitating hydrofoil section shapes were designed at the David W. Taylor Naval Ship R&D Center, using fully nonlinear theory. The foils were built and tested at the California Institute of Technology (C.I.T.), in order to obtain experimental verification of the design-method. This report compares the DTNSRDC predicted foil performance (including wall-effects) with the experimental data of C.I.T. Agreement is good for the lift and moment results, but only at cavitation numbers near or somewhat above →

DD FORM 1 JAN 73 1473 EDITION OF 1 NOV 65 IS OBSOLETE
S/N 0102-LF-014-6601

UNCLASSIFIED
SECURITY CLASSIFICATION OF THIS PAGE (When Data Entered)

389 694

4B

the choked tunnel conditions (which nearly coincide with the design conditions). The drag coefficients are in not as good agreement. Cavity length was difficult to discern during the experiments, thus, only qualitative statements are made in the report on this aspect.

The discrepancy in the drag results could be a consequence of the theory, indicating the necessity for further refinement. However, the difficulty in obtaining accurate two-dimensional drag measurements may have significantly contributed to the disagreement in the drag results.

ACCESSION for
NTIS White Section
DDC Buff Section
UNANNOUNCED
JUSTIFICATION
BY
DISTRIBUTION/AVAILABILITY CODES
Dist. AVAIL. and/or SPECIAL
A

DDC
RECEIVED
DEC 5 1977
D

TABLE OF CONTENTS

	Page
ABSTRACT	1
ADMINISTRATIVE INFORMATION	1
INTRODUCTION	1
THE EXPERIMENTAL MODELS	3
EXPERIMENTAL PROGRAM	13
ANALYTICAL PREDICTIONS PROGRAM	15
DISCUSSION OF RESULTS	17
CONCLUSIONS AND RECOMMENDATIONS	23
ACKNOWLEDGMENTS	28
REFERENCES	29

LIST OF FIGURES

Page

* Figure 1 - Profiles of Prescribed and Model Hydrofoil (for 1039)..... 31

* Figure 2 - Profiles of Prescribed and Model Hydrofoil (for 1040)..... 32

* Figure 3 - Profiles of Prescribed and Model Hydrofoil (for 1041)..... 33

* Figure 4 - Inspection Axes Designation, From Ref. 6..... 34

Figure 5 - Sample Crossplot as Generated by Running the Wall Effects Program (Foil 1039, α = 9.0°)..... 35

Figure 6 - Comparison of Experimental and Predicted Lift Coefficients for 1039, α = 4.941°..... 36

Figure 7 - Comparison of Experimental and Predicted Lift Coefficients for 1039, α = 6.0°..... 37

Figure 8 - Comparison of Experimental and Predicted Lift Coefficients for 1039, α = 9.0°..... 38

Figure 9 - Comparison of Experimental and Predicted Lift Coefficients for 1039, α = 15.0°..... 39

Figure 10 - Comparison of Experimental and Predicted Lift Coefficients for 1040, α = 5.558°..... 40

Figure 11 - Comparison of Experimental and Predicted Lift Coefficients for 1040, α = 7.0°..... 41

Figure 12 - Comparison of Experimental and Predicted Lift Coefficients for 1040, α = 9.0°..... 42

Figure 13 - Comparison of Experimental and Predicted Lift Coefficients for 1040, α = 11.0°..... 43

Figure 14 - Comparison of Experimental and Predicted Lift Coefficients for 1040, α = 15.0°..... 44

Figure 15 - Comparison of Experimental and Predicted Lift Coefficients for 1041, α = 6.571°..... 45

Page

Figure 16 - Comparison of Experimental and Predicted Lift Coefficients for 1041, α = 7.0° 46

Figure 17 - Comparison of Experimental and Predicted Lift Coefficients for 1040, α = 9.0° 47

Figure 18 - Comparison of Experimental and Predicted Lift Coefficients for 1041, α = 15.0° 48

Figure 19 - Comparison of Experimental and Predicted Drag Coefficients for 1039, α = 4.941° 49

Figure 20 - Comparison of Experimental and Predicted Drag Coefficients for 1039, α = 6.0° 50

Figure 21 - Comparison of Experimental and Predicted Drag Coefficients for 1039, α = 9.0° 51

Figure 22 - Comparison of Experimental and Predicted Drag Coefficients for 1039, α = 15.0° 52

Figure 23 - Comparison of Experimental and Predicted Drag Coefficients for 1040, α = 5.558° 53

Figure 24 - Comparison of Experimental and Predicted Drag Coefficients for 1040, α = 7.0° 54

Figure 25 - Comparison of Experimental and Predicted Drag Coefficients for 1040, α = 9.0° 55

Figure 26 - Comparison of Experimental and Predicted Drag Coefficients for 1040, α = 11.0° 56

Figure 27 - Comparison of Experimental and Predicted Drag Coefficients for 1040, α = 15.0° 57

Figure 28 - Comparison of Experimental and Predicted Drag Coefficients for 1041, α = 6.571° 58

Figure 29 - Comparison of Experimental and Predicted Drag Coefficients for 1041, α = 7.0° 59

Figure 30 - Comparison of Experimental and Predicted Drag Coefficients for 1041, α = 9.0° 60

Figure 31 - Comparison of Experimental and Predicted Drag Coefficients for 1041, α = 15.0° 61

Page

Figure 32 - L/D Curves of 1039, 1040, and 1041 at Design Angles of Attack..... 62

Figure 33 - Comparison of Experimental and Predicted Moment Coefficients for 1039, $\alpha = 4.941°$..... 63

Figure 34 - Comparison of Experimental and Predicted Moment Coefficients for 1040, $\alpha = 5.558°$..... 64

Figure 35 - Comparison of Experimental and Predicted Moment Coefficients for 1041, $\alpha = 6.571°$..... 65

Figure 36 - Comparison of Experimental and Predicted Moment Coefficients for 1039, $\alpha = 9.0°$..... 66

* Figure 37 - Axial Velocity Profile Along Balance Port Centerline Viewed Looking into the Direction of Flow..... 67

Figure 38 - Tip Vortex Occurring Betweer Foil Tip and Test Section Window..... 68

Figure 39 - Growth of Cavity On Foil H-1039 with Increasing Angle of Attack, at $\sigma = 0.50$..... 69

Figure 40 - Growth of Cavity On Foil H-1039 with Decreasing Cavitation Number, at $\alpha = 4.94°$.... 70

* Indicates Figures taken from Reference 6

LIST OF TABLES

TABLE 1 - FOIL DESIGNATIONS AND DESIGN VALUES..... 3

TABLE 2 - MODEL NO. 1039, NORMALIZED COORDINATES..... 4

TABLE 3 - MODEL NO. 1040, NORMALIZED COORDINATES..... 5

TABLE 4 - MODEL NO. 1041, NORMALIZED COORDINATES..... 6

* TABLE 5 - MODEL NO. 1039, INSPECTION RECORDS..... 7

* TABLE 6 - MODEL NO. 1040, INSPECTION RECORDS..... 9

* TABLE 7 - MODEL NO. 1041, INSPECTION RECORDS..... 11

* Indicates Tables taken from Reference 6

NOMENCLATURE

		Dimensions
A	Planform area of hydrofoil A = B x C	l^2
B	Span of hydrofoil	l
b', c	Algebraic parameters used in mapping the wall effect case, related to H/ℓ and σ respectively	
C	Chord of hydrofoil	l
C_D	Drag coefficient, $C_D = D/ \frac{1}{2}\rho U_\infty^2 A$	
C_L	Lift coefficient, $C_L = L/ \frac{1}{2}\rho U_\infty^2 A$	
C_M	Moment coefficient, $C_M = M/ \frac{1}{2}\rho U_\infty^2 AC$	
D	Drag force	mlt^{-2}
H	Height of tunnel test section	l
L	Lift force	mlt^{-2}
ℓ	Arc length of foil section shape	l
ℓ_{cav}	Length of cavity from foil leading edge	l
M	Pitching moment, positive when tending to rotate the hydrofoil leading edge upward about an axis taken normal to the longitudinal centerline of the working section through the mid-chord point	ml^2t^{-2}
p_c	Cavity pressure, absolute	$ml^{-1}t^{-2}$
p_v	Vapor pressure of water, absolute	$ml^{-1}t^{-2}$
p_∞	Upstream static pressure of water, absolute	$ml^{-1}t^{-2}$
R_n	Reynolds number, $R_n = (U_\infty C)/\nu$	
U_∞	Upstream velocity of water relative to the foil	lt^{-1}
α	Angle of attack of hydrofoil measured between working section longitudinal centerline and hydrofoil chord line, positive when the leading edge is rotated upward	

ν	Kinematic viscosity of water	l^2t^{-1}
ρ	Density of water	ml^{-3}
σ_{cp}	Cavitation number based on measured cavity pressure $\sigma_{cp} = (p_\infty - p_c)/\frac{1}{2}\rho U_\infty^2$	
σ_{vp}	Cavitation number based on vapor pressure of water $\sigma_{cp} = (p_\infty - p_v)/\frac{1}{2}\rho U_\infty^2$	

ABSTRACT

Three supercavitating hydrofoil section shapes were designed at the David W. Taylor Naval Ship R&D Center, using fully nonlinear theory. The foils were built and tested at the California Institute of Technology (C.I.T.), in order to obtain experimental verification of the design-method. This report compares the DTNSRDC predicted foil performance (including wall-effects) with the experimental data of C.I.T. Agreement is good for the lift and moment results, but only at cavitation numbers near or somewhat above the choked tunnel conditions (which nearly coincide with the design conditions). The drag coefficients are in not as good agreement. Cavity length was difficult to discern during the experiments, thus, only qualitative statements are made in the report on this aspect.

The discrepancy in the drag results could be a consequence of the theory, indicating the necessity for further refinement. However, the difficulty in obtaining accurate two-dimensional drag measurements may have significantly contributed to the disagreement in the drag results.

ADMINISTRATIVE INFORMATION

This work was sponsored by Naval Sea Systems Command under their Ship Performance and Hydromechanics Program, Task area ZF43421001. The report was completed under Work Unit 1-1500-100-10.

INTRODUCTION

Buoyant seagoing vehicles have often been characterized as relatively slow in the spectrum of transportation, the reason being their high resistance to motion due to large wetted surface areas. One solution to this problem has been to use hydrofoils, hydrodynamic lift-producing wings, to lift the vehicle hull out of the water and thus reduce the resistance to motion at higher speeds.

Hydrofoils have some speed limitations of their own. As speed is increased and the pressure is reduced on the low pressure side of the foil, cavitation bubbles begin to appear. The harmful effects of cavitation are: erosion of the foil material, noise from the cavitation bubbles collapsing on the foil surface and reduced lift-drag ratio (L/D). A solution to this problem is to design the foil so that it is completely covered with one large cavitation bubble on its low pressure side, which collapses somewhere aft of the foil surface. This approach is in a sense a concession to reduced L/D ratio but on the other hand does solve the problems of erosion.

The primary variable governing the inception and growth of cavitation is the dimensionless cavitation number,

$$\sigma_{cp} = \frac{p_\infty - p_c}{\frac{1}{2}\rho U_\infty^2}$$

In open water the freestream velocity, U_∞, is the major variant. Experimentation with small scale foils is done in closed variable pressure water tunnels, which introduces a tunnel wall effect on the test data. Design and investigative procedures, and the corrections for the tunnel walls for fully wetted foils have been well established, but analysis of fully cavitating foil data is open to much refinement.

Linear theories have proved inadequate in the design of supercavitating foils and for the prediction of their performance. For this program, three supercavitating hydrofoil sections have been designed using nonlinear theory. The foils have been built by C.I.T. and experimental data were collected in the two-dimensional (2-D) test

section of the C.I.T. variable pressure water tunnel. These data were used at DTNSRDC for comparison with the analytical predictions.

THE EXPERIMENTAL MODELS

Three supercavitating hydrofoils were designed at DTNSRDC. Table 1 shows the foil designations and overall design characteristics.

Table 1

C.I.T. Designation	H-1039	H-1040	H-1041
DTNSRDC Designation	F-4007A	35-235	35-435
σ	0.135	0.135	0.135
α	4.9411°	5.5575°	6.572°
C_L	0.3062	0.3500	0.3500
$(L/D)_{inviscid}$	13.24	9.957	8.87
(ℓ_{cav}/C) free stream	3.644	3.990	3.986

Throughout the rest of this report the foils will be referred to using the C.I.T. designations. Foil 1039 was designed using the theory of Larock and Street[1]* which employs the Tulin single-spiral-vortex model[2] (closed wake). Foils 1040 and 1041 were obtained from the theory of Wu[3] which uses the Roshko[4] wake model (open wake), sometimes referred to as the parallel-plate wake model. The angle α is measured from the nose tail line, and the cavity length is taken as twice the distance to the parallel plates of the wake model for 1040 and 1041. Both theories are fully nonlinear and have been programmed for use as design tools. A report[5] describing the use of these programs for designing

* References listed on page 29

Station: X/C	Surface: Y/C	
	Upper	Lower
0.00	0.000	0.000
0.05	0.013	0.002
0.10	0.022	0.005
0.15	0.029	0.009
0.20	0.037	0.013
0.25	0.044	0.017
0.30	0.051	0.020
0.35	0.057	0.022
0.40	0.063	0.024
0.45	0.069	0.025
0.50	0.074	0.026
0.55	0.080	0.026
0.60	0.084	0.025
0.65	0.089	0.024
0.70	0.093	0.022
0.73*	0.094	0.021
0.75	0.093	0.020
0.80	0.087	0.017
0.85	0.075	0.014
0.90	0.056	0.010
0.95	0.031	0.005
1.00	0.000	0.000

Note: Approximate dimensions taken from a three-foot chord scale drawing

* Point of maximum thickness

TABLE 2 - MODEL NO. 1039; NORMALIZED COORDINATES

Station : X/C	Surface : Y/C	
	Upper	Lower
0.00	0	0
0.05	0.014	-0.001
0.10	0.022	-0.003
0.15	0.030	-0.004
0.20	0.038	-0.003
0.25	0.046	-0.001
0.30	0.053	+0.002
0.35	0.060	0.006
0.40	0.067	0.011
0.45	0.073	0.015
0.50	0.079	0.019
0.55	0.086	0.023
0.60	0.091	0.026
0.65	0.096	0.028
0.70	0.100	0.030
0.72*	0.102	0.030
0.75	0.100	0.030
0.80	0.093	0.028
0.85	0.079	0.025
0.90	0.059	0.019
0.95	0.032	0.011
1.00	0	0

Note: Approximate dimensions taken from a three foot chord scale drawing

* Point of maximum thickness

TABLE 3 - MODEL NO. 1040; NORMALIZED COORDINATES

Station: X/C	Surface: Y/C	
	Upper	Lower
0.00	0	0
0.05	0.015	-0.001
0.10	0.026	0
0.15	0.036	0
0.20	0.044	0
0.25	0.053	0.002
0.30	0.061	0.004
0.35	0.069	0.007
0.40	0.076	0.011
0.45	0.084	0.014
0.50	0.091	0.017
0.55	0.098	0.020
0.60	0.105	0.023
0.65	0.111	0.024
0.70	0.116	0.025
0.71*	0.117	0.025
0.75	0.116	0.025
0.80	0.107	0.023
0.85	0.090	0.020
0.90	0.067	0.016
0.95	0.037	0.009
1.00	0	0

Note: Approximate dimensions taken from a three foot chord scale drawing

* Point of maximum thickness

TABLE 4 - MODEL NO. 1041; NORMALIZED COORDINATES

Survey along axes parallel to span

Station: Z'-Axis in.	Deviation from Initial Value	
	A-Axis in.	B-Axis in.
0.5	.0000	.0000
1.0	.0001	.0000
1.5	.0005	.0000
2.0	.0008	.0001
2.5	.0006	.0002
3.0	.0005	.0002
3.5	.0006	.0001
4.0	.0008	-.0001
4.5	.0010	-.0002
5.0	.0014	-.0002
5.5	.0013	-.0002

TABLE 5 - MODEL NO. 1039, INSPECTION RECORDS

This Table is reproduced directly from Reference 6

Survey along axes parallel to chord

Station X-Axis in.	Upper Surface			Lower Surface		
	Y in.	C-Axis Δ, in.	D-Axis Δ, in.	Y in.	C-Axis Δ, in.	D-Axis Δ, in.
0.05	.0179	-.0001	-.0002	.0012	-.0004	-.0007
0.10	.0313	.0006	.0016	.0029	-.0004	-.0009
0.15	.0426	-.0001	.0009	.0048	.0000	-.0010
0.20	.0530	.0001	.0009	.0069	-.0001	-.0008
0.25	.0630	.0002	.0007	.0092	-.0002	-.0009
0.30	.0727	.0004	.0007	.0017	-.0005	-.0008
0.35	.0822	.0008	.0009	.0144	-.0006	-.0005
0.40	.0914	.0009	.0009	.0172	-.0007	-.0004
0.45	.1004	.0009	.0009	.0201	-.0007	-.0003
0.50	.1092	.0008	.0007	.0231	-.0007	-.0003
0.55	.1179	.0007	.0007	.0263	-.0005	-.0003
0.60	.1263	.0010	.0009	.0296	-.0009	-.0002
0.65	.1346	.0007	.0007	.0330	-.0008	-.0002
0.70	.1428	.0007	.0008	.0366	-.0006	-.0001
0.75	.1509	.0005	.0008	.0402	-.0002	-.0002
0.80	.1588	.0009	.0009	.0439	-.0007	-.0003
0.85	.1667	.0007	.0003	.0477	-.0005	-.0002
0.90	.1745	.0005	.0005	.0515	-.0001	.0002
0.95	.1822	.0008	.0006	.0554	-.0002	.0001
1.00	.1902	.0001	.0004	.0594	.0001	.0001
1.50	.2637	.0003	-.0007	.0999	-.0006	-.0003
2.00	.3299	.0009	.0007	.1298	-.0002	-.0005
2.50	.3904	.0004	.0006	.1481	-.0009	-.0004
3.00	.4462	.0003	.0002	.1559	-.0006	-.0006
3.50	.4972	.0003	.0001	.1537	.0011	-.0009
4.00	.5434	.0008	.0008	.1419	-.0002	-.0004
4.50	.5597	.0006	-.0003	.1206	-.0010	.0002
5.00	.4734	.0004	-.0002	.0899	.0001	-.0001
5.50	.2849	.0007	-.0007	.0498	-.0002	.0008

TABLE 5 - CONTINUED

Survey along axes parallel to span

Station: Z'-Axis in.	Deviation from Initial Value	
	A-Axis in.	B-Axis in.
0.5	.0000	.0000
1.0	-.0002	.0000
1.5	-.0003	.0000
2.0	-.0002	.0000
2.5	-.0003	.0000
3.0	-.0003	.0001
3.5	-.0003	.0001
4.0	-.0002	.0001
4.5	-.0002	.0001
5.0	-.0002	.0001
5.5	-.0001	.0001

TABLE 6 - MODEL NO. 1040, INSPECTION RECORDS

This Table is reproduced directly from Reference 6

Survey along axes parallel to chord

Station X-Axis in.	Upper Surface			Lower Surface		
	Y in.	C-Axis Δ, in.	D-Axis Δ, in.	Y in.	C-Axis Δ, in.	D-Axis Δ, in.
0.05	.0224	.0009	.0010	.0017	-.0008	-.0009
0.10	.0370	.0009	.0010	.0014	.0000	-.0008
0.15	.0497	.0007	.0009	.0003	.0005	-.0003
0.20	.0611	.0001	.0007	-.0014	.0004	.0000
0.25	.0718	-.0005	.0002	-.0034	.0004	-.0006
0.30	.0819	-.0007	.0002	-.0055	-.0007	-.0007
0.35	.0915	-.0005	.0001	-.0076	-.0009	-.0008
0.40	.1009	-.0005	.0001	-.0098	-.0008	-.0008
0.45	.1099	-.0006	.0000	-.0119	-.0009	-.0008
0.50	.1187	-.0007	.0001	-.0138	-.0007	-.0008
0.55	.1273	-.0003	-.0001	-.0156	-.0005	-.0004
0.60	.1357	-.0004	-.0004	-.0172	-.0003	-.0003
0.65	.1440	-.0006	-.0005	-.0186	-.0003	-.0003
0.70	.1522	-.0012	-.0009	-.0198	-.0002	-.0003
0.75	.1602	-.0009	-.0009	-.0207	-.0001	-.0006
0.80	.1682	-.0010	-.0010	-.0214	.0002	-.0003
0.85	.1760	-.0010	-.0010	-.0219	.0002	.0001
0.90	.1838	-.0008	-.0009	-.0221	.0002	.0002
0.95	.1916	-.0011	-.0011	-.0220	.0006	.0004
1.00	.1992	-.0003	-.0009	-.0217	.0002	.0001
1.50	.2739	-.0011	-.0011	-.0054	.0009	.0009
2.00	.3453	-.0011	-.0009	.0283	.0008	.0010
2.50	.4134	-.0002	-.0002	.0709	.0009	-.0009
3.00	.4776	.0009	.0008	.1150	.0009	.0006
3.50	.5365	.0008	.0009	.1527	.0010	.0008
4.00	.5884	.0010	.0009	.1769	.0009	.0006
4.50	.6027	.0001	.0003	.1807	-.0006	.0003
5.00	.5069	-.0001	-.0009	.1576	-.0010	-.0001
5.50	.3037	-.0007	-.0010	.0925	.0008	.0009

TABLE 6 - CONTINUED

Survey along axes parallel to span

Station: X-Axis in.	Deviation from Initial Value	
	A-Axis in.	B-Axis in.
0.5	.0000	.0000
1.0	.0000	.0001
1.5	-.0003	.0002
2.0	-.0002	.0002
2.5	-.0003	.0003
3.0	.0009	.0004
3.5	.0012	.0006
4.0	.0013	.0007
4.5	.0016	.0008
5.0	.0018	.0013
5.5	.0021	.0016
6.0	.0023	.0017
6.5	.0027	.0019
7.0	.0036	.0021
7.5	.0040	.0023

TABLE 7 - MODEL NO. 1041, INSPECTION RECORDS

This Table is reproduced directly from Reference 6

Survey along axes parallel to chord

Station X-Axis in.	Upper Surface			Lower Surface		
	Y in.	C-Axis Δ, in.	D-Axis Δ, in.	Y in.	C-Axis Δ, in.	D-Axis Δ, in.
0.05	.0248	-.0005	-.0003	.0030	-.0024	-.0027
0.10	.0413	-.0009	-.0004	.0043	-.0031	-.0033
0.15	.0557	-.0008	-.0001	.0048	-.0032	-.0034
0.20	.0688	-.0008	-.0001	.0048	-.0033	-.0033
0.25	.0812	-.0010	-.0002	.0044	-.0033	-.0034
0.30	.0928	-.0013	-.0004	.0039	-.0034	-.0034
0.35	.1041	-.0015	-.0006	.0032	-.0033	-.0031
0.40	.1149	-.0015	-.0007	.0021	-.0029	-.0025
0.45	.1254	-.0017	-.0008	.0011	-.0026	-.0023
0.50	.1356	-.0017	-.0007	.0006	-.0028	-.0024
0.55	.1456	-.0017	-.0009	.0002	-.0031	-.0027
0.60	.1554	-.0018	-.0011	-.0002	-.0033	-.0030
0.65	.1650	-.0017	-.0011	-.0007	-.0033	-.0029
0.70	.1745	-.0017	-.0011	-.0012	-.0032	-.0028
0.75	.1838	-.0016	-.0010	-.0015	-.0031	-.0027
0.80	.1930	-.0015	-.0010	-.0016	-.0031	-.0027
0.85	.2021	-.0016	-.0010	-.0015	-.0033	-.0029
0.90	.2111	-.0015	-.0009	-.0012	-.0034	-.0029
0 95	.2120	-.0014	-.0008	-.0009	-.0035	-.0030
1.00	.2288	-.0013	-.0008	-.0005	-.0035	-.0029
1.50	.2146	-.0014	-.0009	.0126	-.0038	-.0032
2.00	.3940	-.0005	-.0002	.0380	-.0037	-.0030
2.50	.4707	.0001	.0001	.0700	-.0035	-.0032
3.00	.5434	.0008	.0005	.1027	-.0034	-.0034
3.50	.6114	.0008	.0002	.1303	-.0032	-.0035
4.00	.6739	-.0008	-.0001	.1472	-.0019	-.0024
4.50	.6916	.0000	-.0003	.1483	-.0014	-.0022
5.00	.5797	.0000	-.0006	.1291	-.0019	-.0028
5.50	.3458	-.0019	-.0027	.0811	-.0021	-.0034

TABLE 7 - CONTINUED

supercavitating hydrofoil sections is in preparation at DTNSRDC. These programs are for designing cambered, two-dimensional, sharp-edged hydrofoil sections at infinite submergence. A method of numerical optimization of lift-to-drag ratio subject to one or several constraints is employed. Structural properties for a section shape are derived by filling in 80 percent of the predicted upper cavity streamline with material, and smoothly fairing the tail section. Filling 80 percent of the cavity leaves a factor of safety in the prediction of the upper streamline. See Figures 1 through 3 for the section shapes of the subject foils. These three models were deliberately chosen to lie in a range of C_L where tunnel wall effects would be quite small, i.e. $0.30 < C_L < 0.50$.

Fabrication of the foils was part of the C.I.T. contract.[6] Accuracy was emphasized in fabrication, with tolerances of ± 0.0005 inch (1.27×10^{-5}m) along the Z-axis and ± 0.001 inch (2.54×10^{-5}m) per side, see Figure 4 for axis designation. The foils were fabricated from 17-4 PH steel, hardened to the H900 condition. Each foil was polished in the direction of flow to a surface finish of 32×10^{-6} inch (8.13×10^{-7}m) average. Tables 2 through 4 are normalized coordinates of the foils. Inspection records for the as-built foils are presented in Tables 5 through 7. See Reference 6 for more detailed information.

EXPERIMENTAL PROGRAM

The experiments were conducted in the high speed water tunnel at the Graduate Aeronautical Laboratories, California Institute of

Technology (GALCIT). The facility is a closed circuit tunnel where pressure can be varied independently of water velocity.[6] For this experiment, the newly constructed 30 inch two-dimensional working section as proposed in Reference 7, was used. Mounting procedures for the foils as well as instrumentation for data collection are discussed thoroughly in Reference 6.

The data collected consists of lift force, drag force, moment about center chord, photographs of cavitation, and measured cavity pressure when possible. A run consisted of collecting data for one angle of attack while holding Reynolds number constant over the following range of cavitation numbers: σ_{vp} = 3.00, 2.00, 1.50, 1.0, .90, .80, .70, .60, .50, .45, .40, .35, .30, .25, .20, .15, .10. The test range in most cases was limited to a cavitation number larger than 0.10, due to choking of the tunnel and large unsteady forces on the experimental equipment. Angles of attack investigated were: α = -1°, 0°, 1°, 2°, 3°, 4°, 5°, 6°, 7°, 8°, 9°, 11°, 13°, 15°, and design angle of attack. At design angle of attack each foil was run at Reynolds numbers of 1.03×10^6, 1.80×10^6, and 2.06×10^6. The highest Reynolds number, corresponding to 40 ft/sec (12.192 m/s), was omitted from the experimental procedure for the other angles of attack.

The numerical data as received by DTNSRDC from C.I.T. are presented in Tables in Reference 6. Corrections were made for the effects of the model and support weight, vertical buoyancy and clear tunnel fairing disk drag. No tunnel boundary effects or other corrections have been made to the data. The photographic data have been returned to DTNSRDC, mostly in

the form of negatives. The experimental force and moment values have been reduced to the usual coefficient forms of C_L, C_D, and C_M, as defined in the NOMENCLATURE. One important note to mention, is that the numerical value of the moment coefficient as presented in Reference 6 is incorrect due to a unit error, and must be divided by 12 to obtain the correct C_M.

ANALYTICAL PREDICTIONS PROGRAM

The nonlinear theory has been programmed[8] and is commonly referred to as the wall-effect program. The theory used in the wall-effect program is expected to be valid at choked conditions and for some range of cavitation numbers higher than choked conditions. Full cavitation, with the cavity length equal to one chord or greater, is a necessary condition for the comparison of theory and experiment. The wall-effect program was therefore run for cavitation numbers ranging from zero to one for several angles of attack. Choked conditions, both experimental and predicted, usually fell between $\sigma_{vp} = 0.1$ and $\sigma_{vp} = 0.3$ while a full chord length of cavity is in most cases questionable above $\sigma_{vp} = 1.00$.

The procedure used in running the program is to generate a cross plot between the internal or input parameters b', c and the external or output parameters ℓ/H, σ, for each foil section shape. A sample plot is shown in Figure 5. First b' is set to its maximum value for each c, and the line corresponding to infinite stream operation is drawn, along which σ varies for each input choice of c, while $H/\ell = \infty$. Then b' is set to

its minimum value for each c, and the line corresponding to the choked flow case is drawn. In that case both the values of H/ℓ and the choking cavitation number σ are determined by the choice of c, while the cavity length always remains infinite in the tunnel. No wake model is needed for this case.

In the geometry of the present experiment, H/ℓ is approximately equal to 5. The program has been modified from the original form presented in Reference 8 so that, given a fixed value of the internal parameter c and an initial value of b', it searches automatically for the value of b' that will make ℓ/H the required value. This is the finite cavity length case. Thus starting with c on the choked line and increasing its value generates data points of C_L, C_D, and C_M for increasing σ, with ℓ/H held constant. These values may be compared with the experimental data. A very accurate starting value of b' must be given in the data input for the search to work properly when c is near the choked case, but this value can be read easily from the already completed choked flow case curve. This modification has reduced the amount of computer time necessary to generate each curve of C_L vs. σ.

The program as described in Reference 8 computes a moment coefficient about the leading edge. The data from C.I.T. has the moment coefficient taken about center chord. Hence, the wall effect program has been modified to compute the moment coefficient corresponding to the C.I.T. data.

DISCUSSION OF RESULTS

The scope of the experiment and the time and cost of running the wall effect program have made it impractical to plot and analyze all of the data. All three foils were analyzed at several angles of attack as follows: 1039, α = 4.94°, 6°, 9°, 15°; 1040, α = 5.56°, 7°, 9°, 11°, 15°; 1041, α = 6.57°, 7°, 9°, 15°. The selection of design and higher angles of attack to be used for comparisons were made after reviewing the photo negatives of the experiment. There is some question as to whether there might have been some wetted surface area on the suction-side leading edge of some of the foils at design and lower angles of attack. Full cavitation, i.e. a cavity length greater than one and full topside cavity coverage, is a necessary condition for a meaningful comparison of the experimental data with the wall effect prediction.

As explained in the text, only the foil H1039 could be run at close to its design conditions of α and σ. The limitation of the minimum testing cavitation number σ_* is due to tunnel blockage by the large models, which had they been cut to a shorter chord, would have been subject to manufacturing errors and to twisting in the fixed span tunnel. To the design condition of H1039, namely α = 4.94° and σ = 0.135, the closest measurement is at α = 4.94° and σ = 0.160, taken at a tunnel speed of 40 ft/sec (12.192 m/sec). Photos taken at this condition seem to show a full cavity above the foil, springing from the leading edge but having a very minimal clearance thickness, and showing a few streamers from the leading edge, of undetermined origin. The cavity termination is

beyond the range of the camera, being more than 2.1 chordlengths from the leading edge. At the next highest σ at which there is a photograph, namely $\sigma = 0.20$ in Figure 40, the cavity termination is approximately 3.2 chordlengths downstream from the leading edge. These numbers might be cautiously compared with the design value under infinite stream conditions at $\sigma = 0.135$, which was 3.6 chordlengths, from Table 1, using the single-spiral vortex wake model. When the analysis program is run for H1039, with wall effects present, the choking condition is predicted at $\sigma_* = 0.1349$, with $C_L = 0.29612$. (That this value of σ matches the design value for infinite stream condition is purely coincidental.) Under these choking conditions the predicted cavity length is infinite, and no wake model is required.

The leading edge cavity on H1040 at design $\alpha = 5.56°$ and $\sigma = 0.20$ and 0.25 (compared to design value $\sigma = 0.135$) is much fuller than that of H1039 and the clearance height is larger and more readily discernible over the leading edge. The leading edge streamers are not visible; however the upper cavity wall appears to break into turbulence at about ½ chord from the leading edge. Again the termination is off the photo scale.

On the foil H1041 at design angle $\alpha = 6.57°$ and $\sigma = 0.25$ and 0.30 compared to design value $\sigma = 0.135$, the leading edge cavity resembles that of H1039, namely a full cavity seems to be present, but there are narrow streamers emanating from the leading edge which may indicate regions of partial wetting, and the cavity clearance height appears to be very slight, although termination is again off-scale.

Both predicted results and experimental data for lift and drag coefficients, have been plotted versus cavitation number. Results are shown for cavitation number based on vapor pressure of water and the cavitation number based on measured cavity pressure, when available. The cavity pressure was measured through an orifice in the tunnel wall approximately 3 inch (.0762 m) aft of the trailing edge of the foil. Thus a cavity length of greater than 1.5 chord was required before any cavity pressure reading could be taken. This accounts for the limited amount of cavitation number measurements based on cavity pressure.

Figures 6 through 18 show the lift coefficient versus cavitation number, Figures 19 through 31 show the drag coefficient versus cavitation number, Figure 32 shows the lift to drag ratio, including viscous effects, while Figures 33 through 36 compare the moment coefficients. Some deviation from the planned experimental program was necessary at the lower cavitation numbers, in most instances due to tunnel choking, or because of large unsteady loads on the force balance. The predicted choked cavitation number, for $H/\ell = 5$, is indicated on the figures. The major problem arising from tunnel choking was that two of the foils, 1040 and 1041, could not be tested at their design cavitation numbers. Foil 1039 was tested at design conditions with good results. It should be noted that the observed cavity length in this condition is probably longer than it would be under infinite stream conditions.

There is some reservation about the reliability of the cavitation number measurements, based on cavity pressure. The values of σ_{cp} do seem to display normal expected behavior at very low cavitation number. That

is, the computed σ_{cp} is slightly less than σ_{vp}, at the very low cavitation numbers, but its value becomes questionable as σ_{vp} is increased. Figures 13 and 24 are good examples of the scatter in σ_{cp}.

The experimental lift coefficient is in good agreement with predictions at the lower cavitation numbers. Errors derived from the force balance could range from ± 2 percent at low lift coefficients of 0.2, down to ± 0.5 percent at higher lift-coefficients of 1.2. The presence of a tunnel side wall boundary layer as indicated in the velocity profile of Figure 37, could tend to lower the actual measured lift coefficient since it was not accounted for in the experimental data. Another source of error could arise from the tip clearance between the free end of the hydrofoil and the plexiglass window of the tunnel. Photographs in Figure 38 show a tip vortex between the free end of the foil and the window. If pressure equalization does occur through this clearance, and it appears in the pictures that it does, it would lower the experimental C_L as well. Both these error sources are not included in the estimate but are thought to be quite small.

The range in which good agreement prevails in the lift coefficients seems to vary with angle of attack. Increasing angle of attack produces larger cavities at somewhat higher cavitation numbers and a wider range of good agreement between the experimental data and predictions. Figure 39 shows the growth of cavities with increasing angle of attack at constant σ; while Figure 40 shows the growth of the cavity with decreasing cavitation number at a constant angle of attack.

The drag data do not show as good agreement with predictions as do the lift data. The best results are at the lowest cavitation numbers and

at higher angles of attack. The wall effect program is a potential flow calculation and therefore does not include any drag due to skin friction. An estimate[9] of the skin friction coefficient for the wetted (lower) surface has been made for a chord Reynolds number of 1.02×10^6, and added to the predicted drag (including wall effect) as shown in the figures. Again it is suspected that the drag coefficient as experimentally measured might be slightly lower than expected since no account is taken for the presence of the tunnel side wall boundary layers. Experimental measuring error for the drag coefficient could run from ±3 percent at the low $C_D = 0.030$, to ±1.5 percent at the higher $C_D = 0.300$. There is a large tare force correction on the mounting cylinder when drag is measured in the water tunnel. The drag curves have a tendency to approach a hump at lower cavitation numbers than do the lift curves, possibly explainable by a re-entrant jet from the short cavity impinging on the foil material.

A lift-to-drag ratio curve is presented in Figure 32. This curve compares each foil at its design angle of attack over a range of cavitation numbers. The predicted curves include an estimate of skin friction drag for this comparison.

Foil 1040 is in closest agreement with prediction, with a 9 percent disagreement at $\sigma_{vp} = .2$. The regime of valid comparisons in Figure 32 is in the lowest cavitation number range, near choked tunnel conditions and up to a cavitation number of 0.4, wherein longer cavities are to be expected. All three L/D curves take on an increased slope at $\sigma \approx 0.4$ due mostly to the premature leveling off of the drag data.

Figures 33 through 36 are moment coefficient curves. The moment curves are consistent with the rest of the data presented so far, in that they display better agreement at lower cavitation numbers, at which the cavity is large. Figure 36 demonstrates that the range in σ of good agreement is extended somewhat by increasing angle of attack.

Another source of discrepancy may be evident at this point. The predicted moment coefficient is computed using an analytical pressure distribution on the foil. The calculation of pressure distributions for this type of foil are still in need of further refinements, in the sense that they depend on the wake model when σ is large and hence may contribute to the disagreement of Figures 33 through 36. Furthermore, the actual magnitudes of the moment coefficient about the center chord are small so that percentage errors are magnified. A quick calculation of center of pressure on the foils can be made by dividing the moment by the lift. For foil 1039, at $\sigma_{vp} \simeq 0.16$, the center of pressure calculation produces an 11.5 percent error between predicted and experimental data for center of pressure location. This is considered to be good agreement for predictions of this kind.

Froude numbers based on the foil chord length ranged from 5 to 10 in these experiments. Figure 23 of Larock and Street[10] indicates that gravity effects would be negligible in this range of Froude numbers, and therefore no accounts of gravity effects have been considered here.

CONCLUSIONS AND RECOMMENDATIONS

The nonlinear theory shows good promise for use in designing and predicting force and moment data of supercavitating foils. The best results occur at choked or near choked tunnel conditions, where the long cavity-length ensures that the choice of cavity wake model is immaterial. The range of good agreement is enlarged somewhat by increasing angle of attack.

In examining the data it is difficult to conclude whether the errors are the fault of the experiment or of the non-linear theory and program used. The program is weak in the following areas: the wake model is not of the highest quality, the numerical integrals must have their domain predefined, and the convergence rate of necessity must be used as the goodness criterion, since convergence cannot be a priori determined. The experimental set-up is weak in these areas: the wall boundary layers cannot be prevented from passing over the model, the effect of the tip clearance gap is not known, there is a large tare force on the drag which must be removed from the data, the cavity pressure measuring port is too far behind the foil, and the model is subject to twist from the applied pitching moment. The effect of most of these can be readily assessed except that of the tip clearance gap, which needs further study to determine its effect on the data. This is however one of the finest water tunnels available in terms of the steadiness of flow, and the size of working section.

Questionable cavity pressure measurement is another area of interest. One possible solution might be to install a pressure

transducer on the upper surface of the foil. This would allow a much wider range of cavity pressure measurements, and also remove the need to purge water from the system as is presently required.

The comparisons between experimental and predicted drag coefficients are in poorer agreement than those for lift and moment. The experimental drag, in most cases, began to level off and peak somewhere between σ_{vp} = 0.6 and 1.0. This phenomenon could have been caused by a re-entrant jet forming behind the short cavities at these cavitation numbers.

The predictions made with the wall effects program indicate that wall effects increase minutely with increasing angle of attack, for these particular highly cambered lifting sections, which were chosen partly for that quality. In the general case of the flat plate (i.e. uncambered) supercavitating hydrofoil, however, the percentage wall effect on the lift coefficient increases with <u>decreasing</u> angle of attack, although the absolute magnitude of ΔC_L due to presence of tunnel walls decreases in that case.

The selection of two different tunnel test speeds over which the force curves of C_L vs. σ were measured allows an assessment of the combined Froude, Weber, and Reynolds number effects on the measured force coefficients. The discernible trend of the C_L values to be reduced slightly at the lower test speed is consistent with a Froude number effect (see for example the theoretical data in Reference 10). The Weber number is thought to affect primarily the shape and texture of the cavity, which was not measured directly in this experiment. The effect of a reduction in Reynolds number might have been to increase the C_L ever

so slightly by thickening the lower surface boundary layer, but supercavitating hydrofoil force coefficients are notably insensitive to angle of attack variations (so long as a cavity is maintained) and this tiny effect is surely lost in the experimental scatter. None of these variations can currently be considered in the wall effects program, which uses potential flow analysis. The addition of the gravity effect would be most desirable, at the reduced Froude numbers at which model experiments are carried out; however, the wall effects program in dealing with infinite or very long cavities near the choked condition would then require a wake model to rejoin the free streamlines even at $\sigma = \sigma_*$. It is not clear how this would correspond to physical reality. A more likely improvement to the program would be to add the shape of the downstream diffuser to the downstream tunnel section, rather than considering the tunnel walls to be infinitely long and parallel as at present. Then the cavity would close naturally in the pressure rise, and the consideration of gravity effects under choked conditions would not be inconsistent with the physical situation.

The tendency of the measured force coefficients to agree better with the predictions at higher angles of attack is probably best explained by the longer cavities existing on the models under that condition. This reduces the size of the plates of the wake model needed to account for the short cavity. The parallel plate wake model is not generally reputed for accuracy at large cavitation numbers although during its development it was compared with other wake models with reasonable success. Under the typical tunnel conditions matching the

infinite stream σ, the cavity is generally long, and the wake model selection less critical. At the low angles of attack, there is always the possibility of partial topside wetting, which for these streamlined models probably raises the lift coefficient slightly. Narrow topside streamers can be seen in the photos of H1039 and H1041 at design angle of attack, though it is not absolutely clear that the upper surface is wetted within them.

Similarly the better agreement of the lift slope $\frac{dC_L}{d\sigma}$ at the larger angles may be explained by the smaller length of the wake model required when the model cavity is longer. This number is completely dependent on the choice of wake model type, and in fact would be an excellent choice of experimental measurement with which to evaluate the wake models themselves, since the number seems to be highly insensitive to tunnel wall effects.

With respect to the overall length of the cavities, which in some photographs appear short, it should be pointed out that each of these three models resulted from a design optimization study to optimize the lift-drag ratio for a particular lift coefficient and section modulus, while keeping the cavitation number constant. Because the section drag in potential flow is quite simply dependent on the cavity cross section, the optimization of the L/D tends to produce smaller and therefore shorter cavities at the fixed cavitation number. In particular for H1040 and H1041, designed with the parallel plate wake model, in infinite stream, the plates, which represent the wake, were approaching quite close to the model as the L/D was increased, even at the $\sigma = 0.135$

corresponding to 80 knot, non-ventilated operation. Clearly the choice of a ventilated system would remove this constraint, allowing a design cavitation number of $\sigma = 0.05$ at the same speed, (see Reference 11) for which the cavity length would be much longer. However though this would allow further optimization of the L/D of a structurally constrained foil section, the overall lift to drag ratio of a three-dimensional strut-foil system might not change much due to higher drag demands of a ventilating strut. The possibility of operating airfoil shaped struts at those speeds does not seem to have been seriously considered.

In this two-dimensional experiment, no attempt has been made to correlate the observed cavity length with the theoretical prediction of the cavity length because

a) The parallel plate wake model does not lend itself to easy definition of the cavity length. Is it the distance to the plates, or twice that distance, as used in some early reports (Reference 12)?

b) The visual observation of the experimental cavity does not precisely define its length, since the region of cavity collapse is unsteady and turbulent.

C) The design of the structurally constrained hydrofoil model is actually driven by the height of the cavity wall above it, so long as the cavity collapses anywhere downstream of the foil (plus possible annex). Therefore the proper measurement to concentrate upon is the height, not the length. In this regard References 13 and 14 may be of interest.

ACKNOWLEDGMENTS

Thanks for help and suggestions in reviewing this report should be given to Dr. Michael B. Wilson. The foil section H1039 was designed by Mr. Donald H. Moore. The Figures 1-3 were prepared by Mr. A. Roper, and report physical preparation was by Mrs. Marjorie Reyes.

REFERENCES

1. Larock, B.E. and Street, R.L., "Cambered Bodies in Cavitating Flow - A Nonlinear Analysis and Design Procedure," Journal of Ship Research, Vol. 12, No. 1 (Mar 1968).

2. Tulin, M.P., "Supercavitating Flows - Small Perturbation Theory," Journal of Ship Research, Vol. 7, No. 3 (Jan 1964).

3. Wu, T.Y., "A Free Streamline Theory for Two-Dimensional Fully Cavitated Hydrofoils," California Institute of Technology H L Report 21-17 (Jul 1955).

4. Roshko, A., "A New Hodograph for Free Streamline Theory," NACA TN 3168 (1964).

5. Baker, E.S., "Selection of Supercavitating Section Shapes," DTNSRDC Report (in preparation).

6. Ward, T.M., "Report on Water-Tunnel Tests of Three Hydrofoils Having Very Sharp Leading Edges in Fully-Wetted and Cavitating Flows," GALCIT Report HSWT-1124 (May 1976).

7. Kiceniuk, T., "A Two-Dimensional Working Section for the High Speed Water Tunnel at the California Institute of Technology," C.I.T. H L Report E-108.1011 (Jul 1964).

8. Baker, E.S., "Analytical Prediction of Wall Effect on Fully Cavitating Lifting Foils, Using Nonlinear Theory," NSRDC Report No. 3688 (Nov 1972).

9. Hadler, J.B., "Coefficients for International Towing Tank Conference 1957 Model-Ship Correlation Line," DTMB Report No. 1185 (Apr 1958).

10. Larock, B.E. and Street, R.L., "A Nonlinear Theory for Fully Cavitating Flows Past an Inclined Flat Plate," Technical Report No. 64 (Jun 1966).

11. Holling, H., Baker, E., and Rood, E., "Experimental Evaluation of the Performance of the TAP-1 Supercavitating Hydrofoil Model at 80 Knots," NSRDC Report 4681 (Jul 1975).

12. Wade, R.B., "Water Tunnel Observations on the Flow Past a Plano-Convex Hydrofoil," California Institute of Technology, Report E-79-6, Pg. 34 (Feb 1964).

13. Johnson, V.E., "Theoretical and Experimental Investigation of Supercavitating Hydrofoils Operating Near the Free Water Surface," NASA Technical Report R-93 (1961).

14. Altmann, R.J., "Measurement of Cavity Shapes Above Ventilated Hydrofoils," Hydronautics, Inc., Report TR 457-1 (Nov 1965).

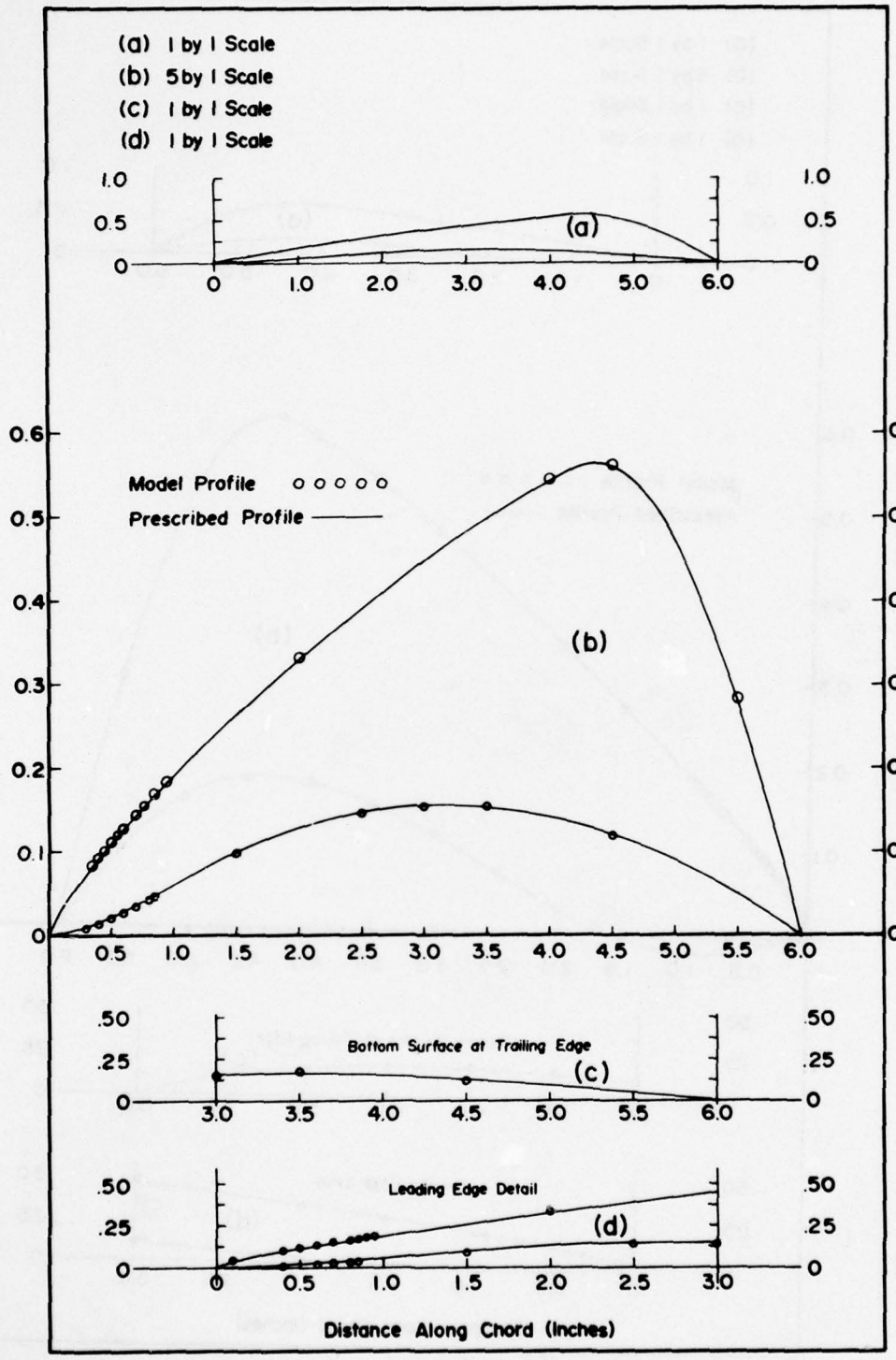

Fig. 1 — Profiles of Prescribed and Model Hydrofoil
(for 1039)

This Figure is reproduced directly from Reference 6

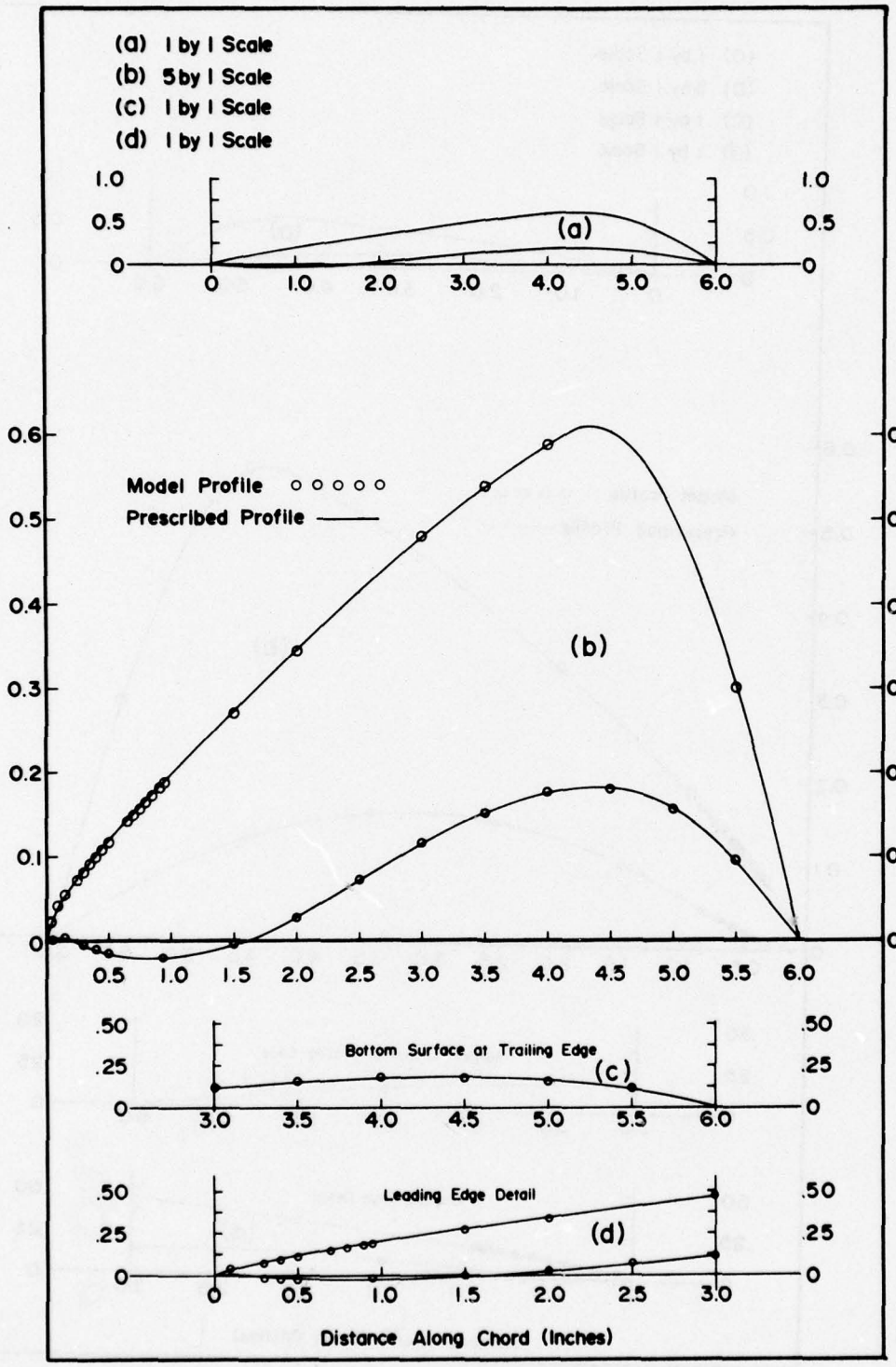

Fig. 2—Profiles of Prescribed and Model Hydrofoil
(for 1040)

This Figure is reproduced directly from Reference 6

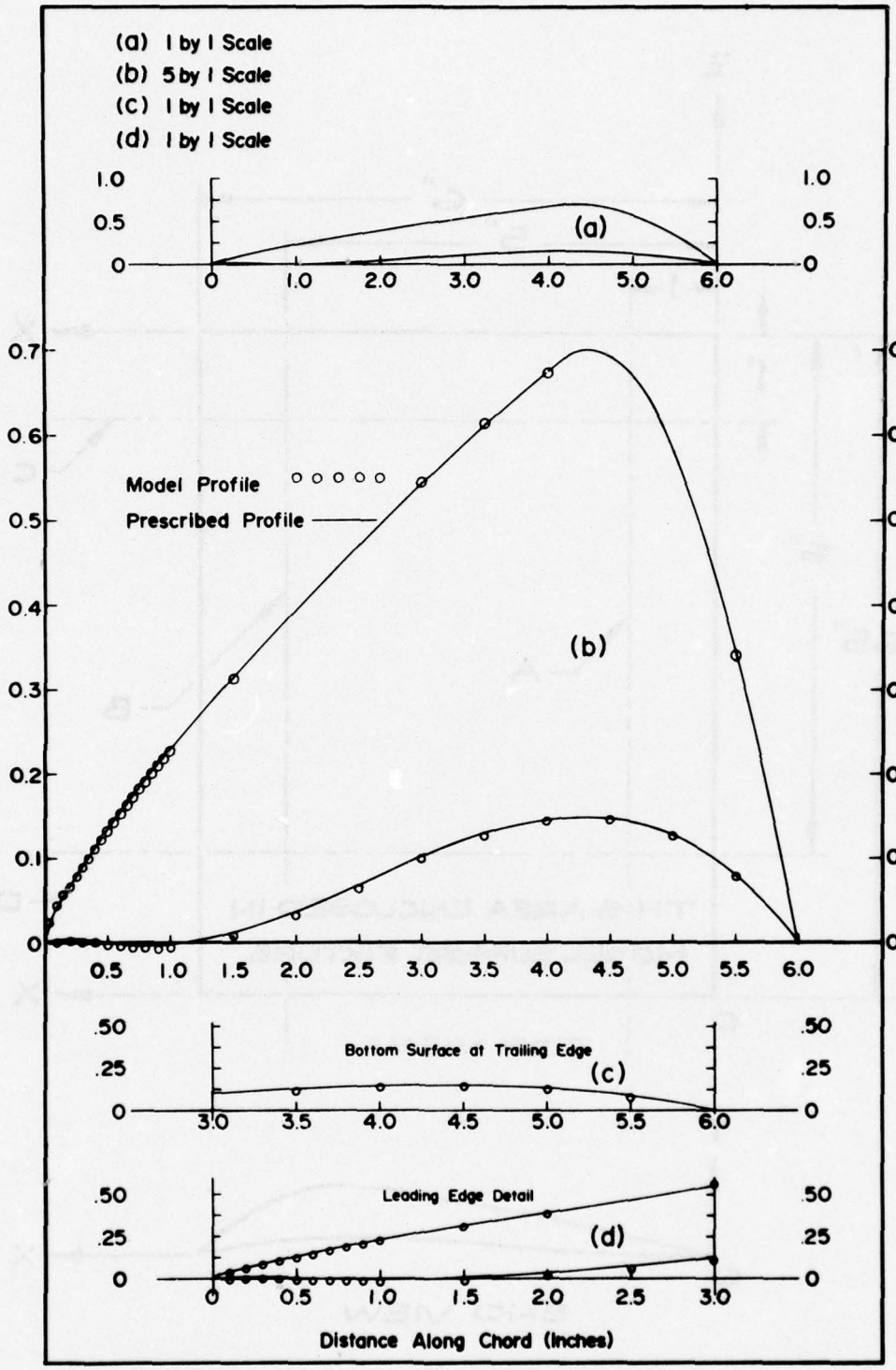

Fig. 3 — Profiles of Prescribed and Model Hydrofoil
(for 1041)

This Figure is reproduced directly from Reference 6

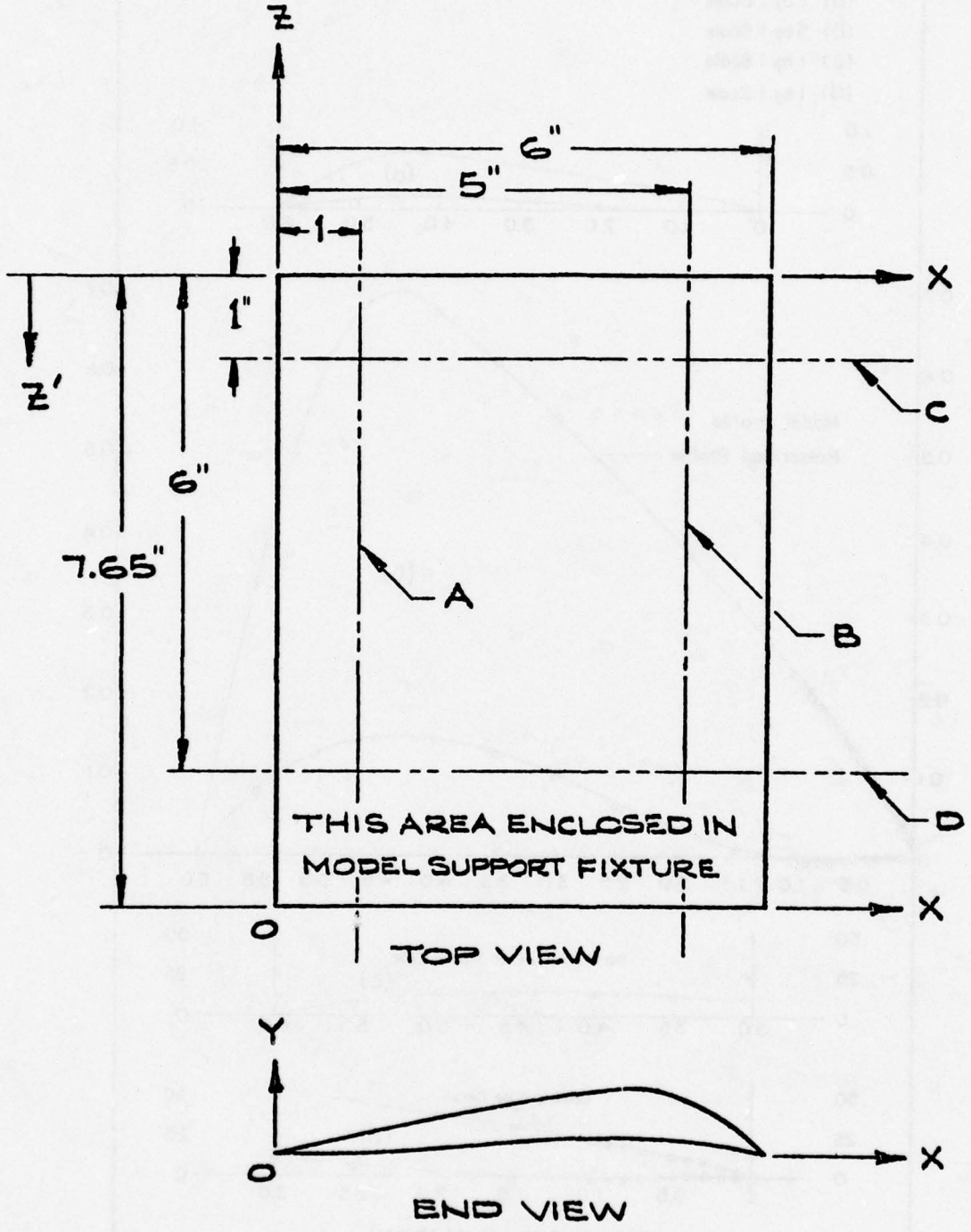

Fig. 4 - Inspection Axes Designation, From ref. 6

This Figure is reproduced directly from Reference 6

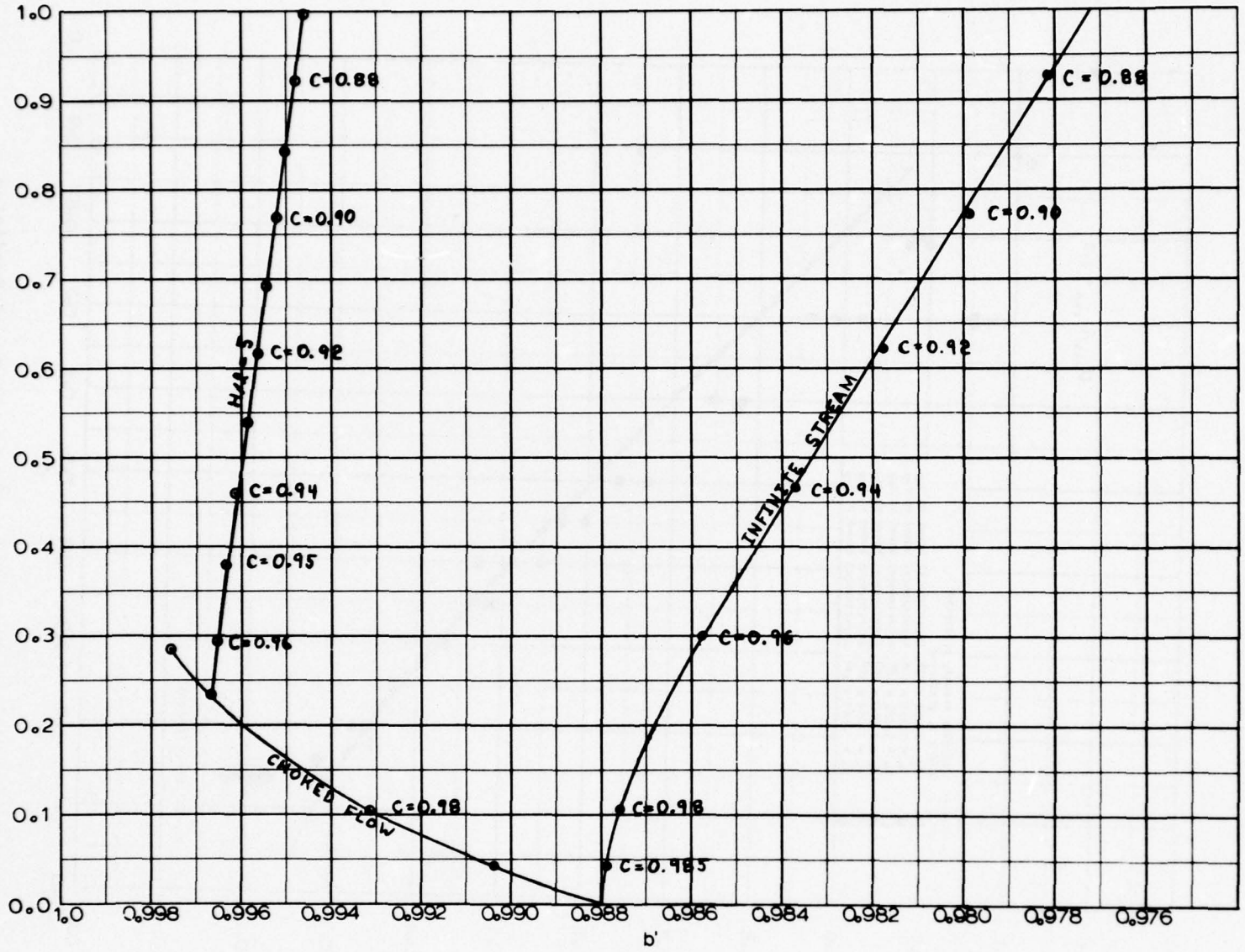

Fig. 5 - Sample Crossplot as Generated by Running the Wall Effects Program (Foil 1039, α = 9.0°)

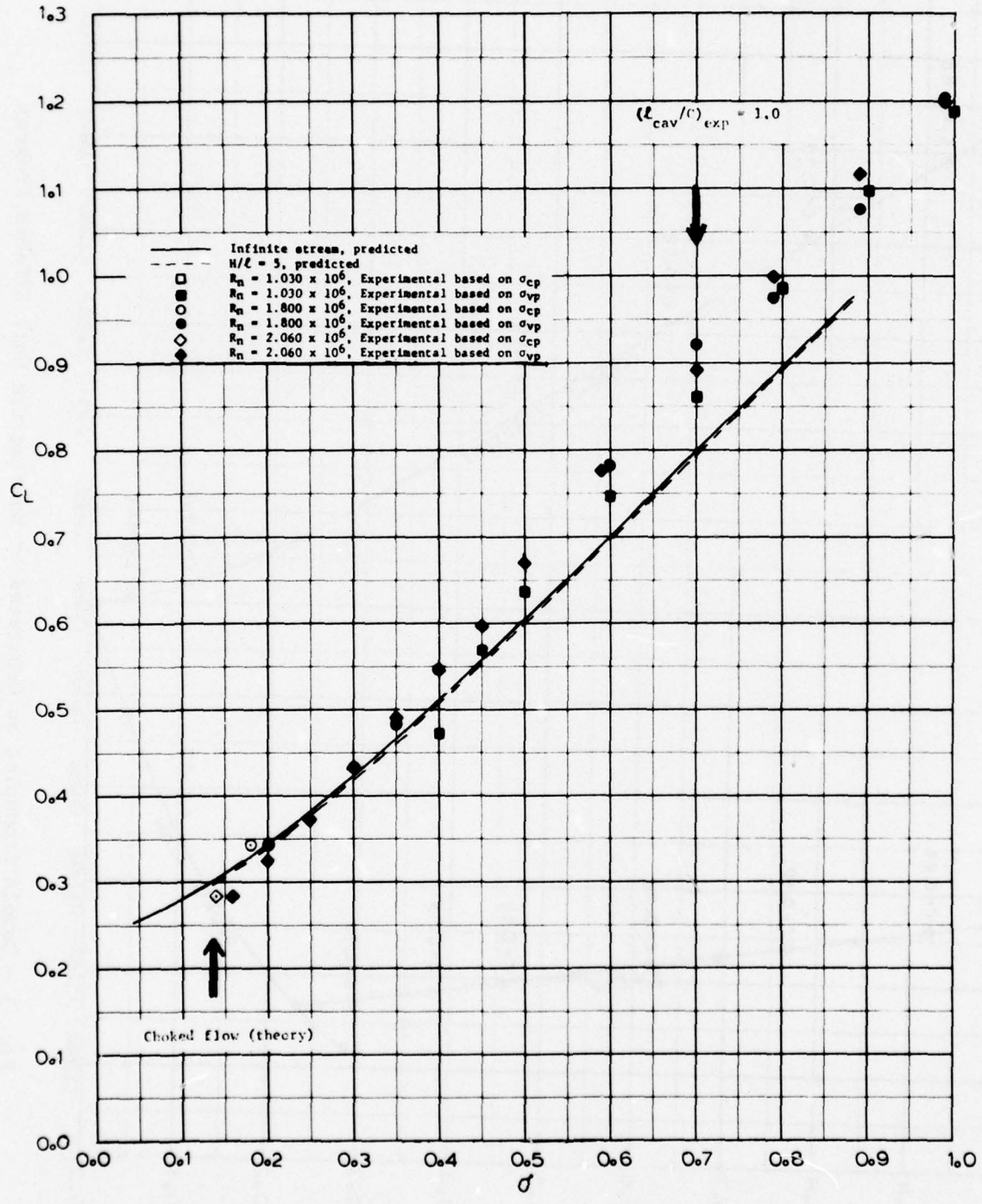

Fig. 6 - Comparison of Experimental and Predicted Lift Coefficients for 1039, $\alpha = 4.941^{\circ}$

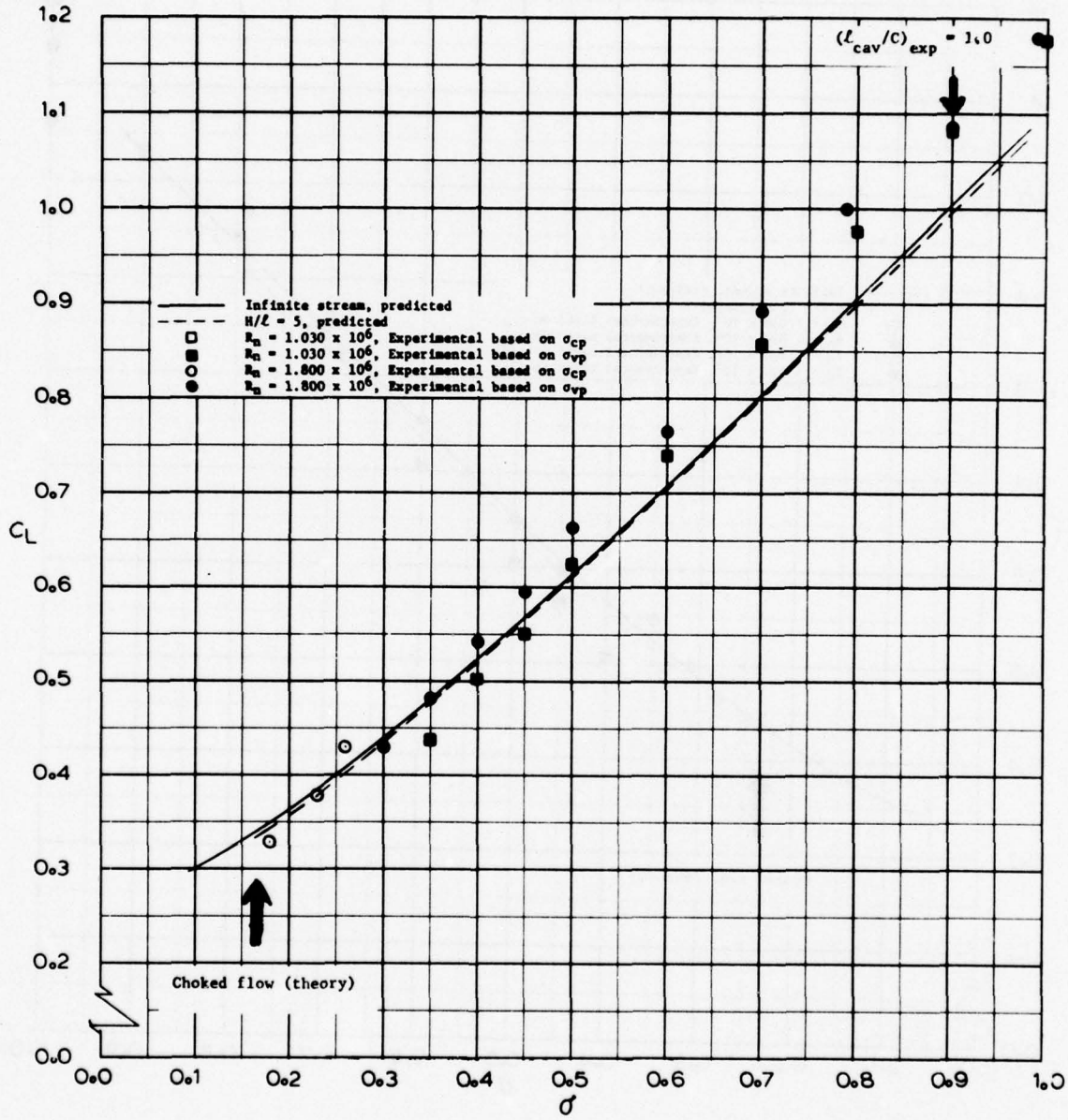

Fig. 7 - Comparison of Experimental and Predicted Lift Coefficients for 1039, α = 6.0°

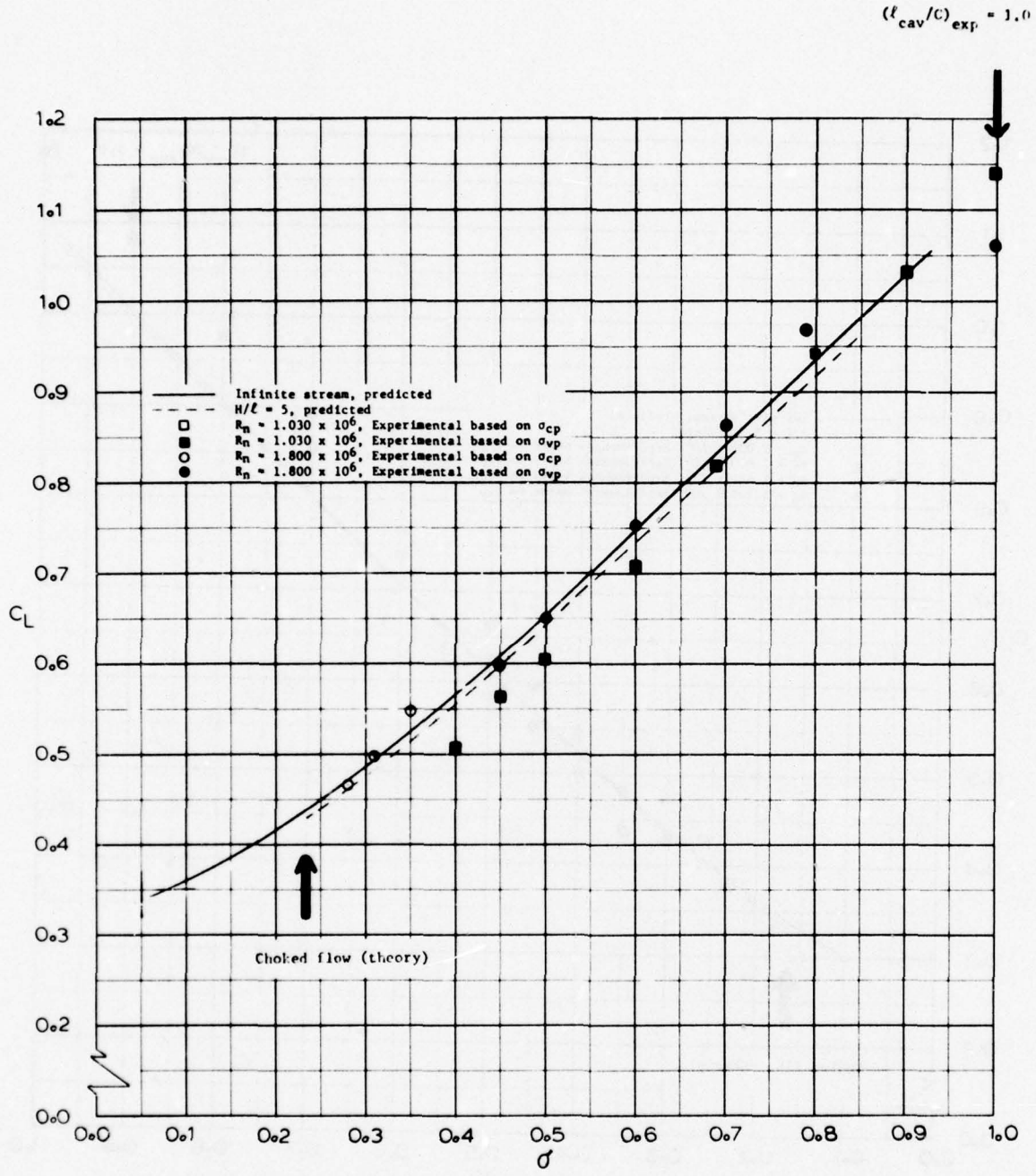

Fig. 8 - Comparison of Experimental and Predicted Lift Coefficients for 1039, $\alpha = 9.0°$

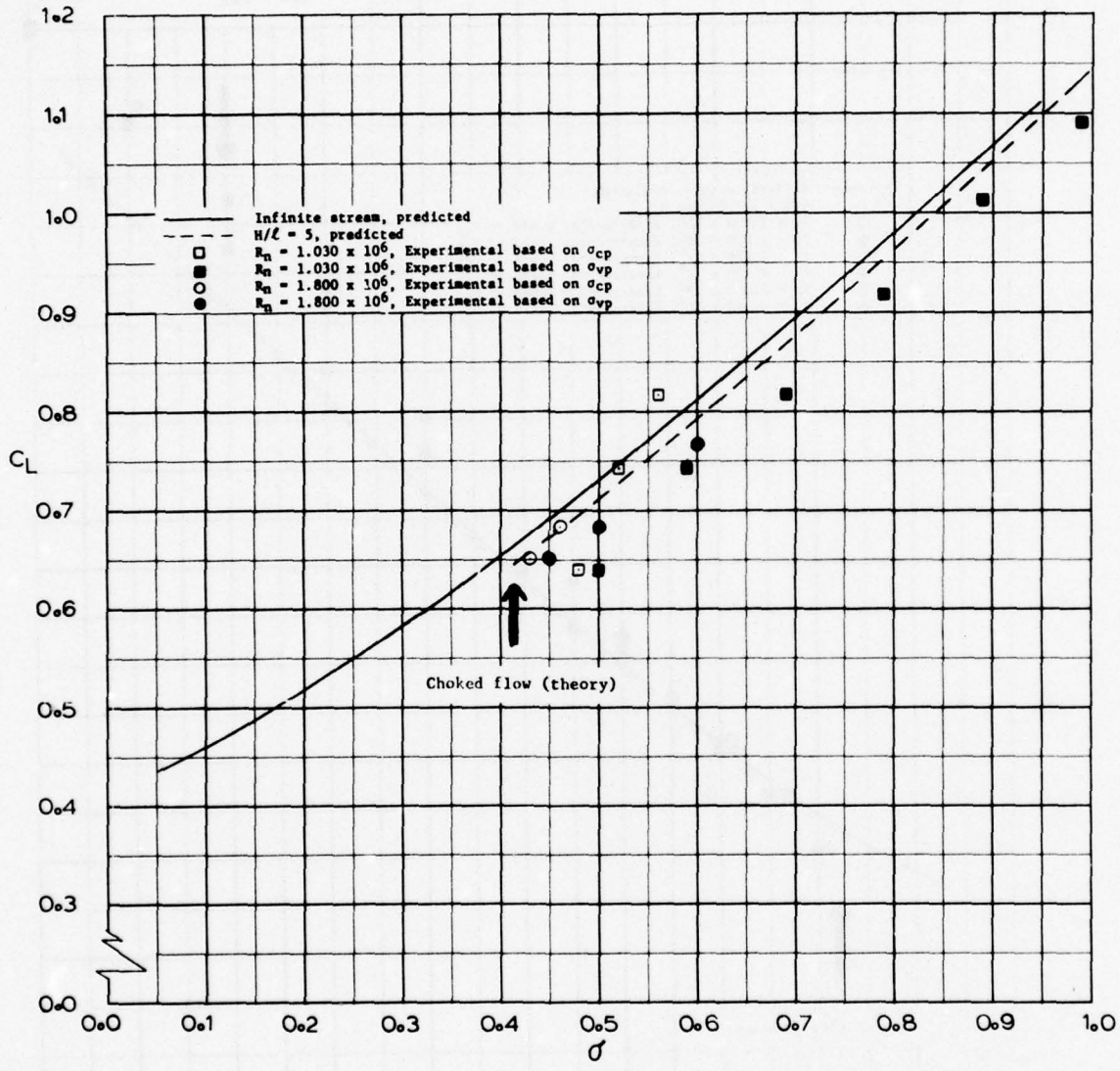

Fig. 9 - Comparison of Experimental and Predicted Lift Coefficients for 1039, $\alpha = 15.0^\circ$

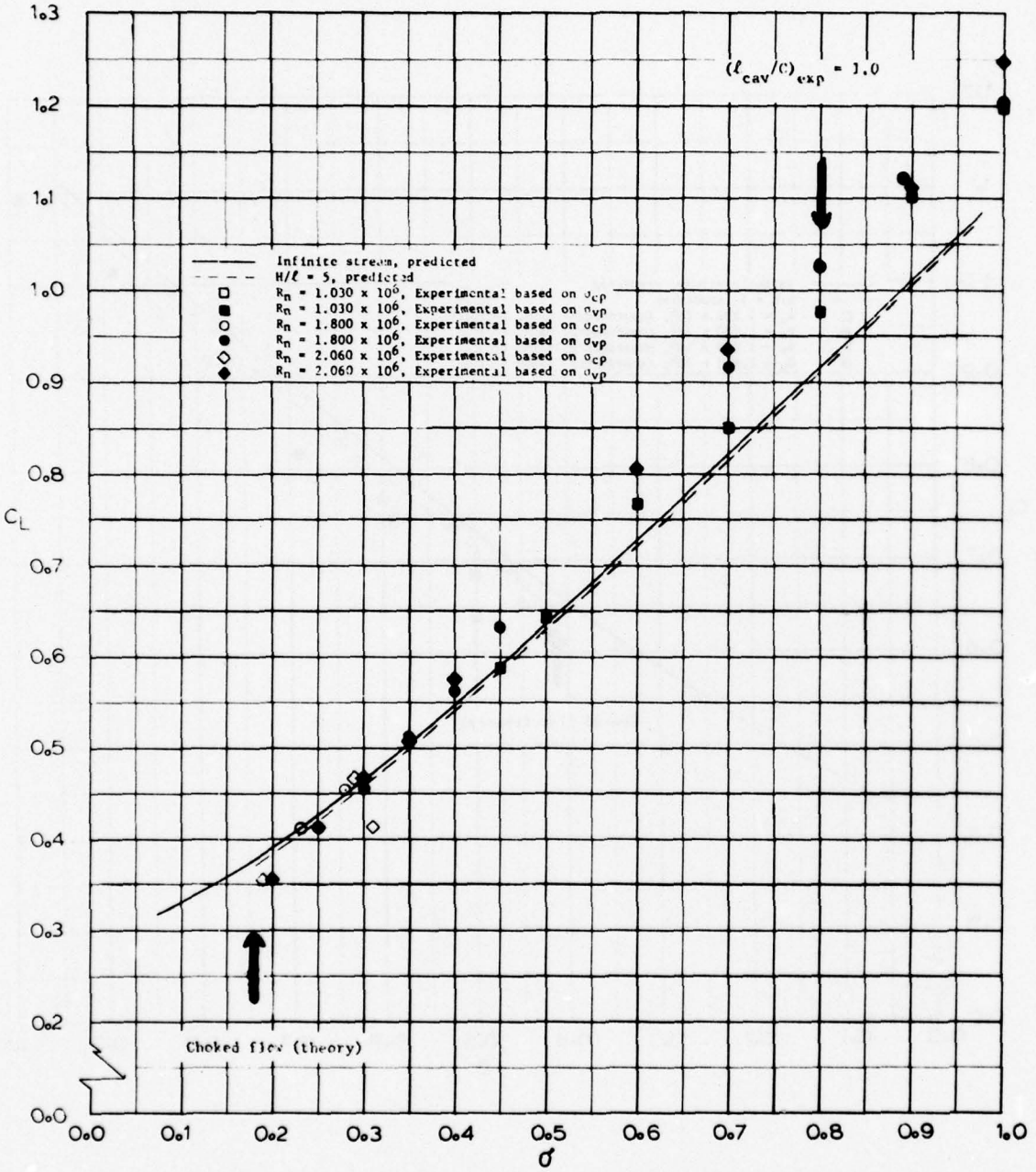

Fig. 10 - Comparison of Experimental and Predicted Lift Coefficients for 1040, $\alpha = 5.558^{\bullet}$

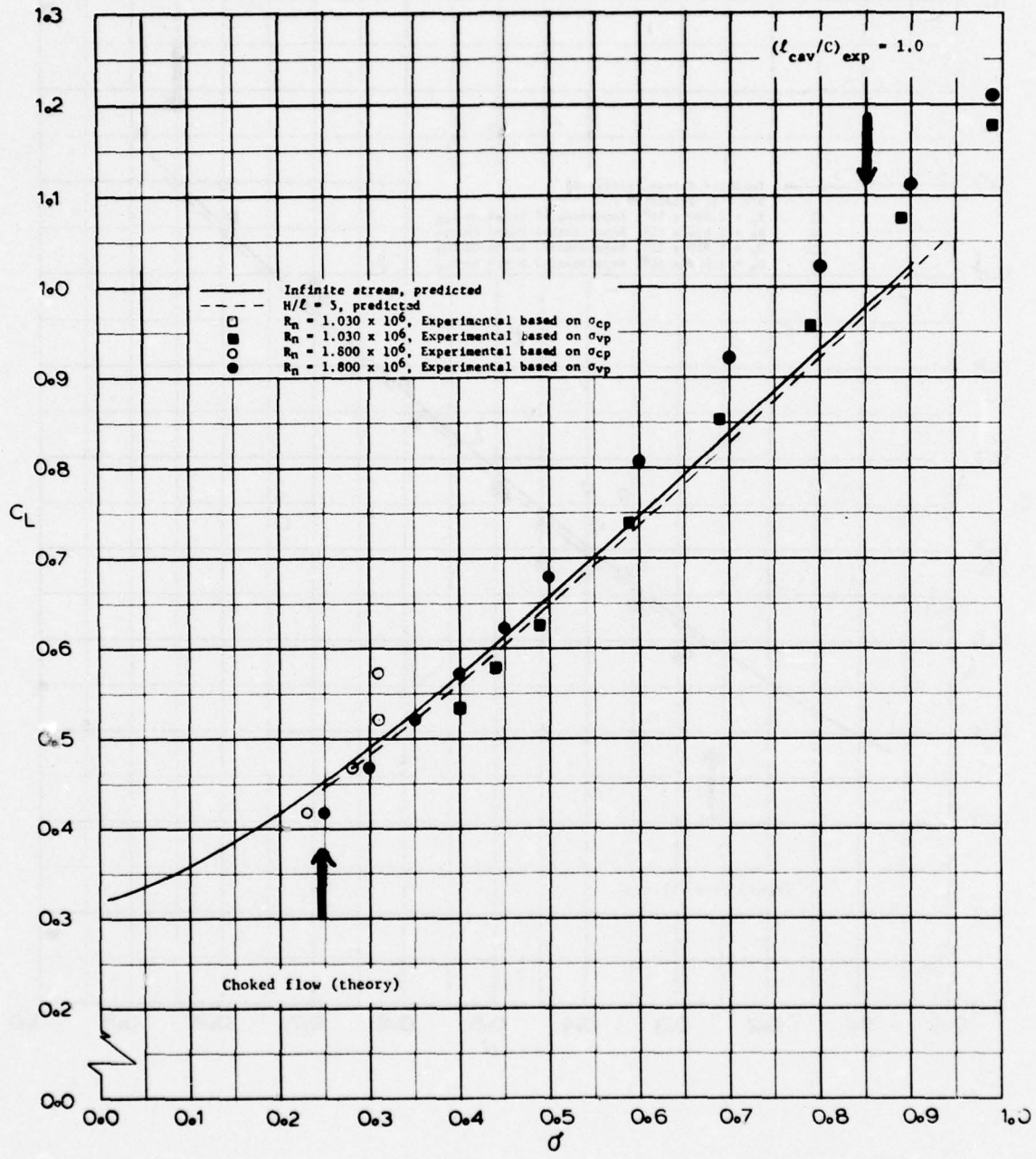

Fig. 11 - Comparison of Experimental and Predicted Lift Coefficients for 1040, α = 7.0°

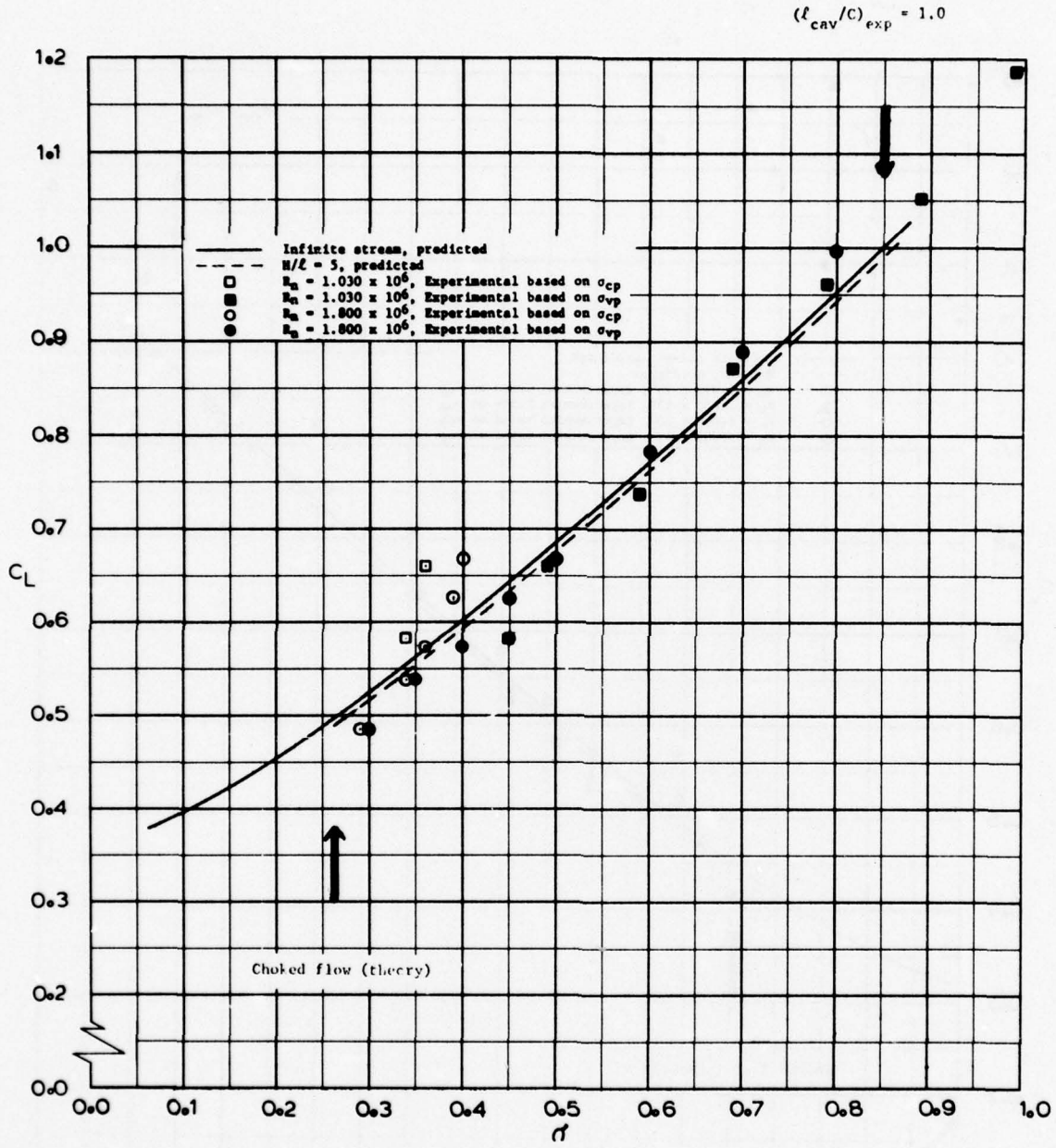

Fig. 12 - Comparison of Experimental and Predicted Lift Coefficients for 1040, $\alpha = 9.0^{\circ}$

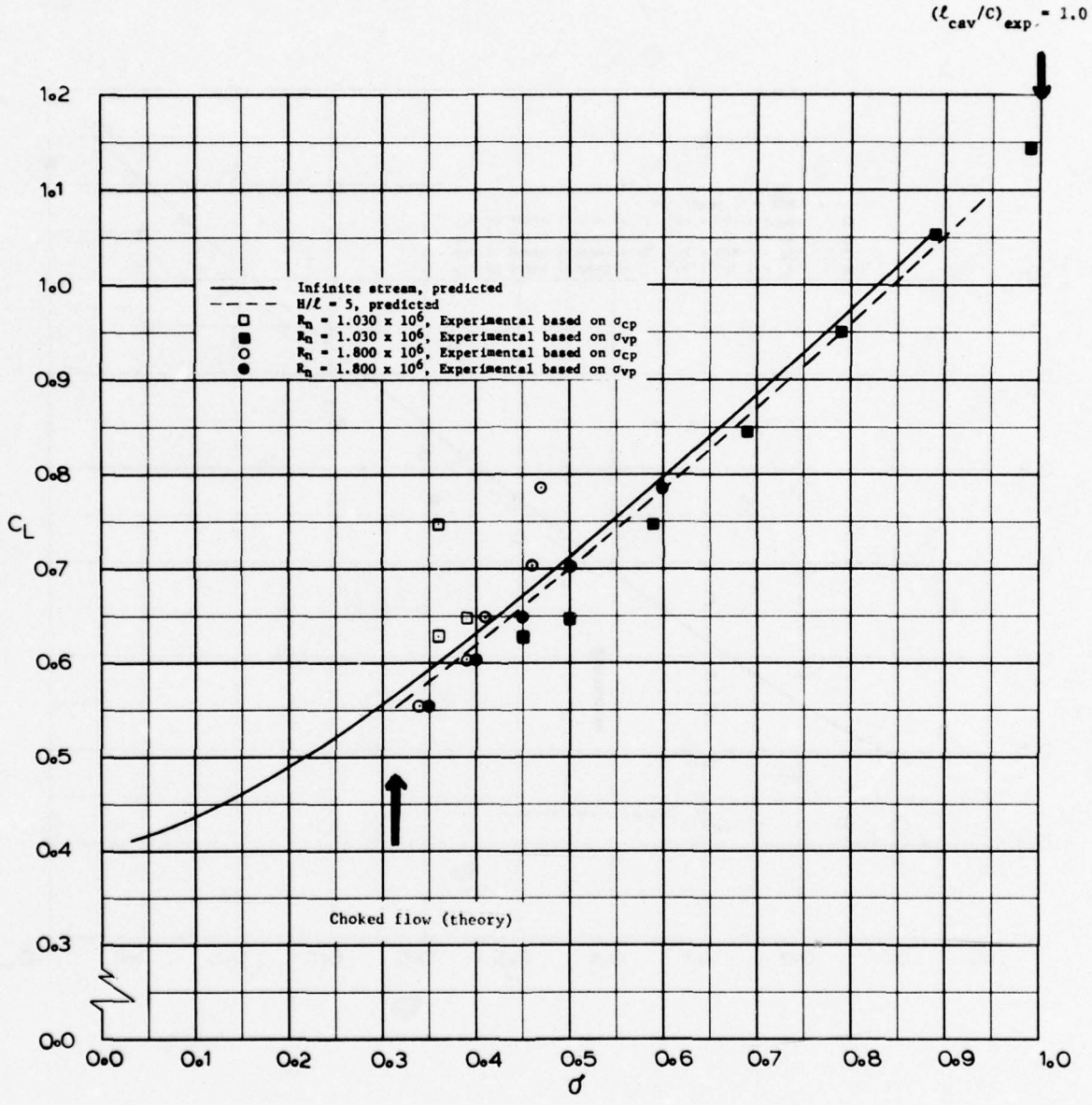

Fig. 13 - Comparison of Experimental and Predicted Lift Coefficients for 1040, α = 11.0°

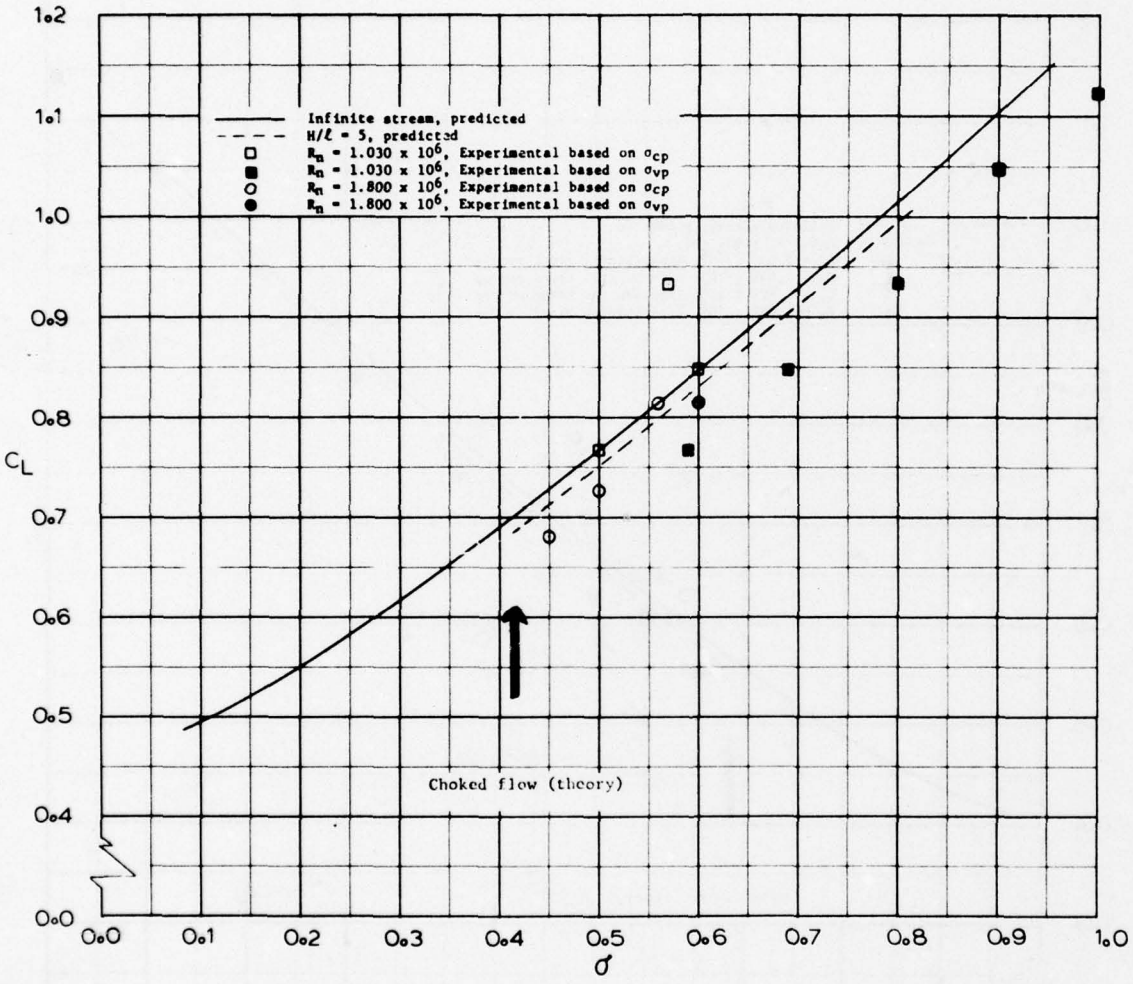

Fig. 14 - Comparison of Experimental and Predicted Lift Coefficients for 1040, α = 15.0°

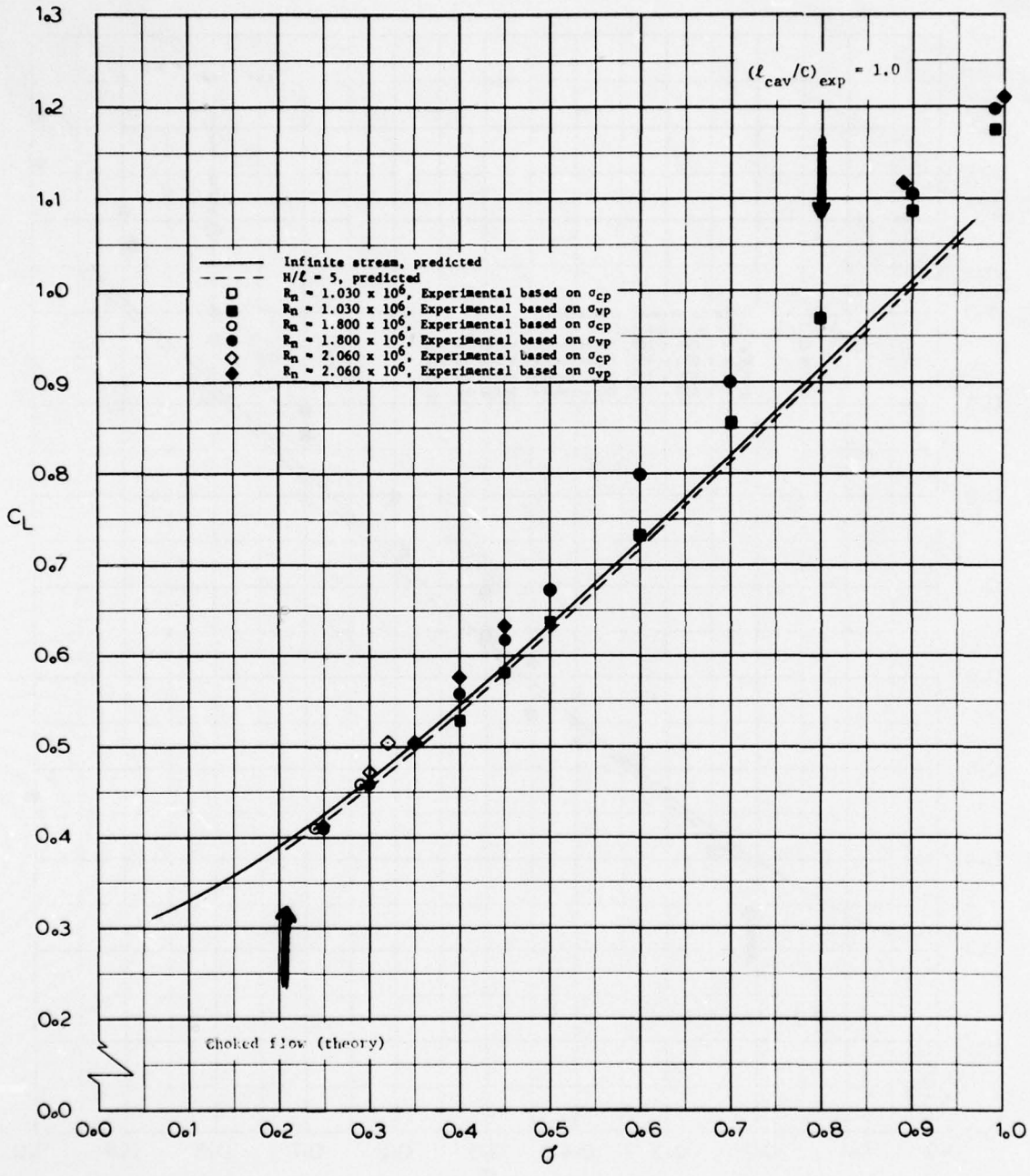

Fig. 15 - Comparison of Experimental and Predicted Lift Coefficients for 1041, $\alpha = 6.571°$

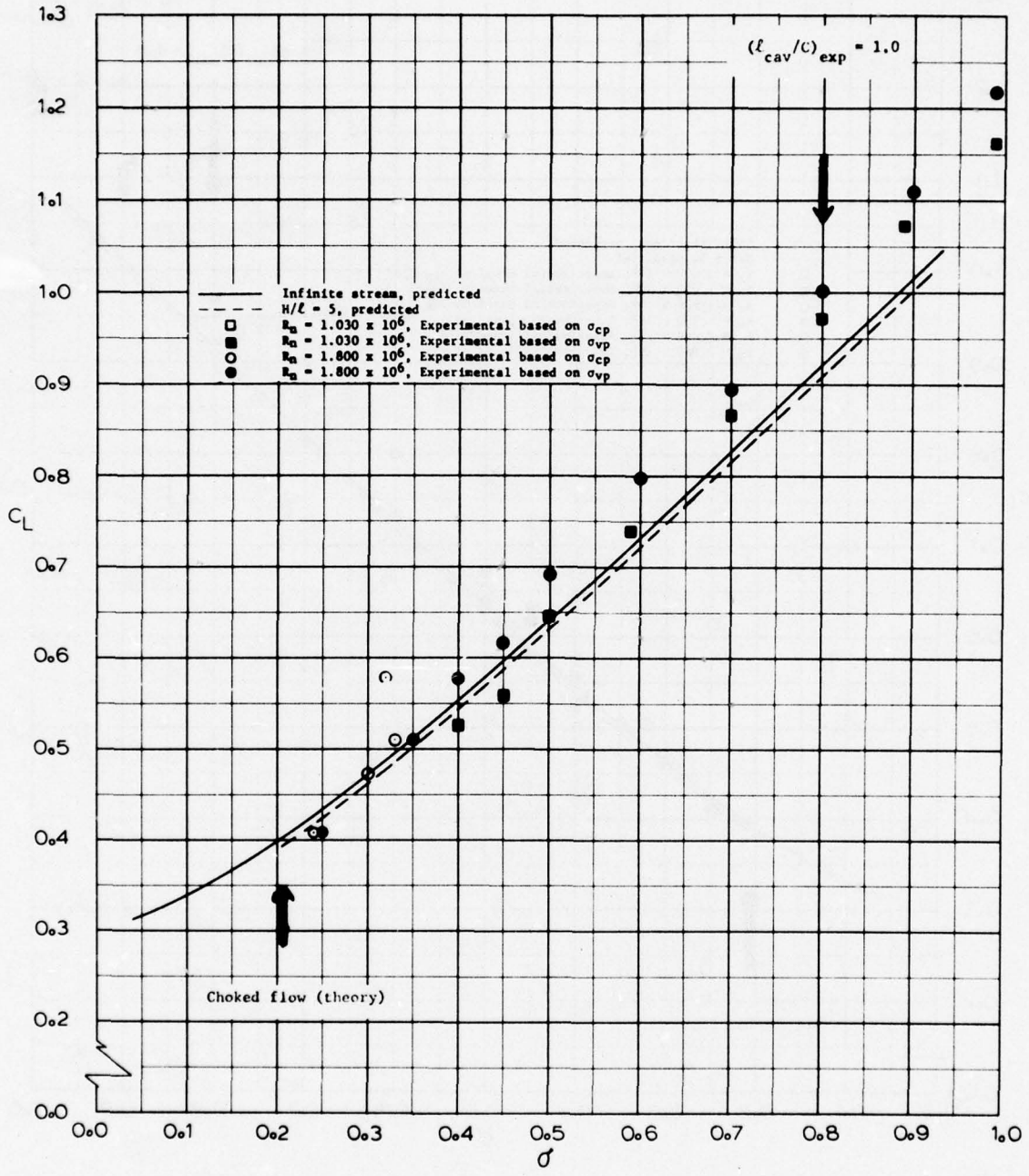

Fig. 16- Comparison of Experimental and Predicted Lift Coefficients for 1041, α = 7.0°

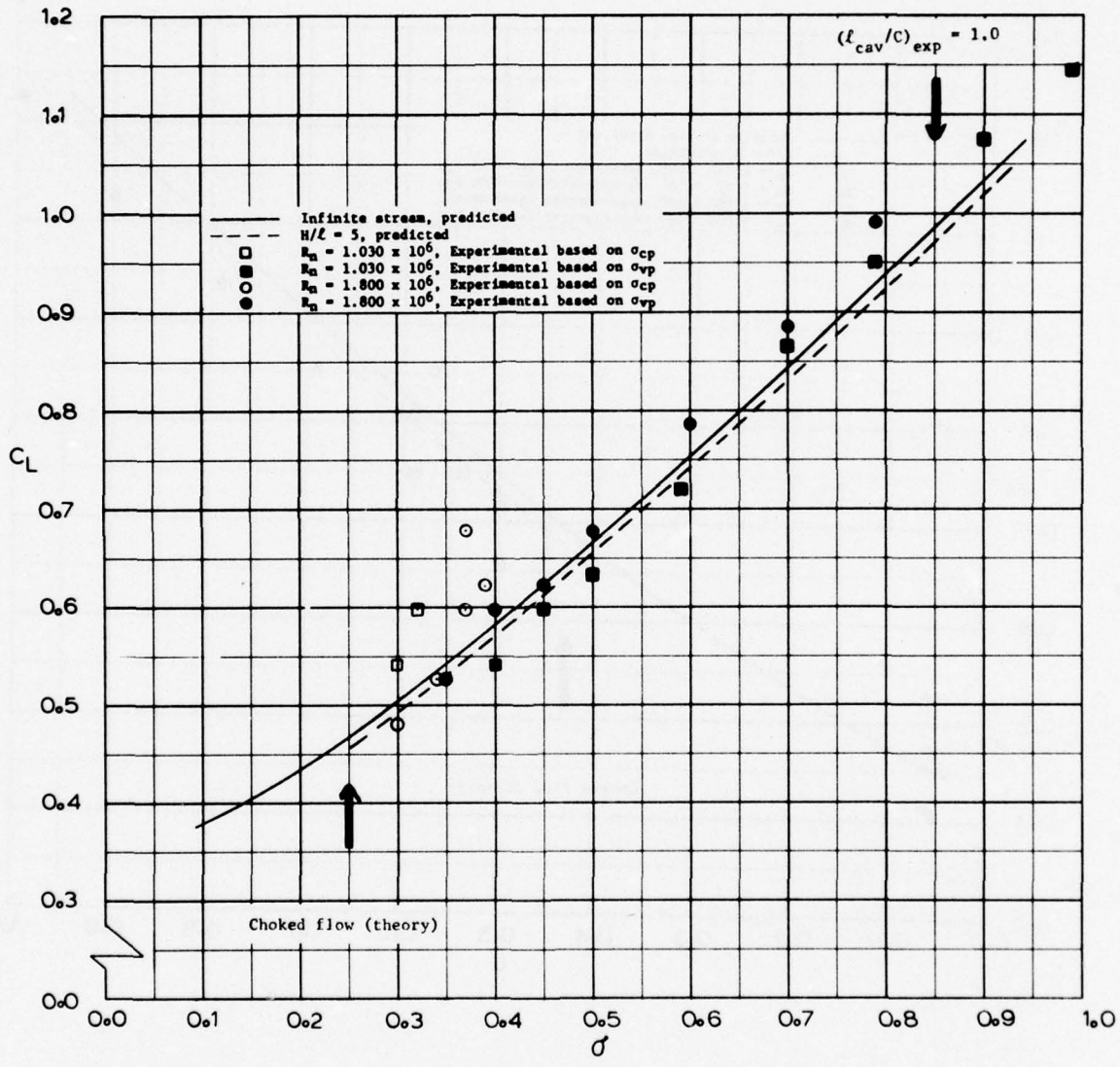

Fig. 17 - Comparison of Experimental and Predicted Lift Coefficients for 1041, α = 9.0°

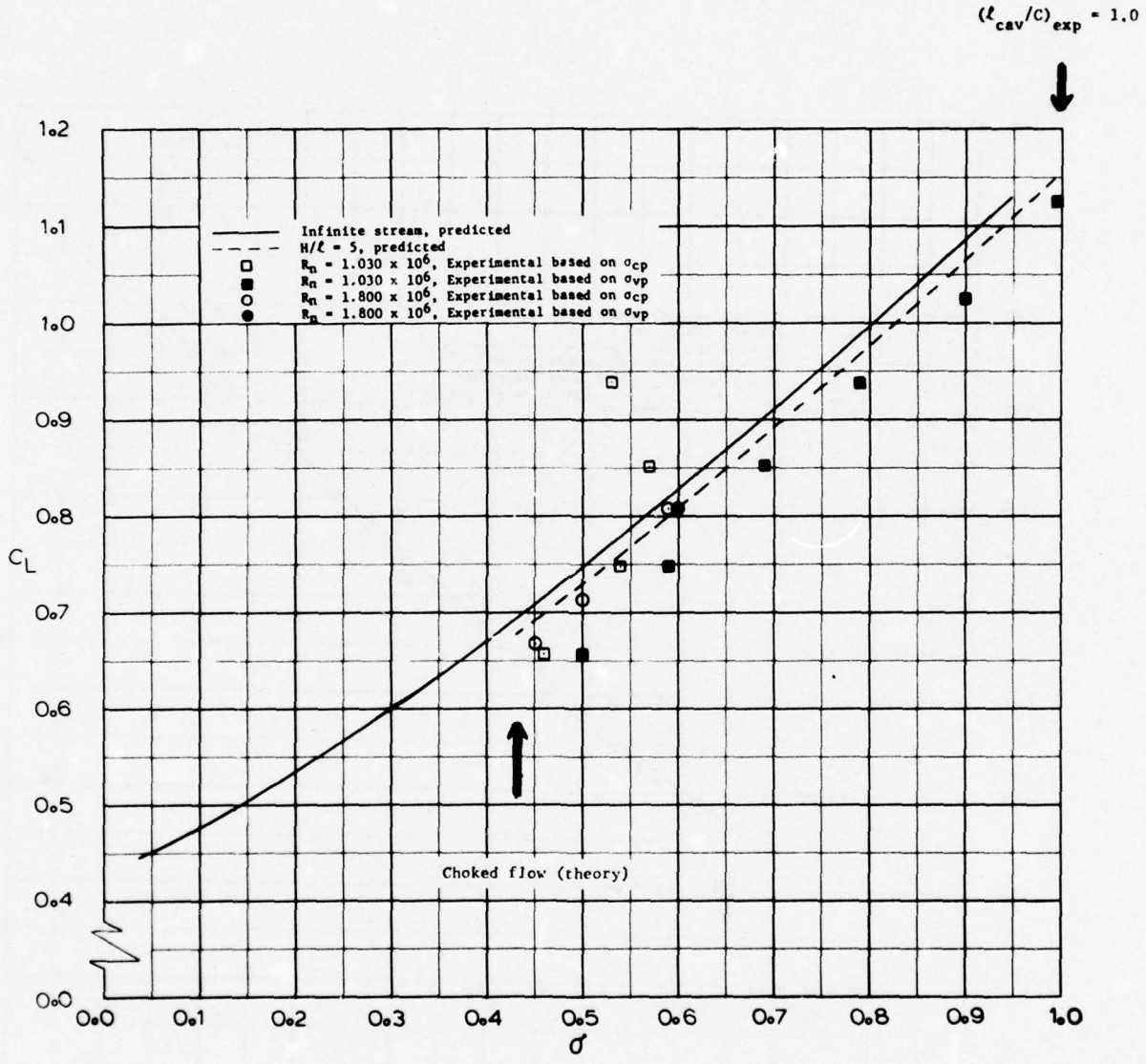

Fig. 18 - Comparison of Experimental and Predicted Lift Coefficients for 1041, α = 15.0°

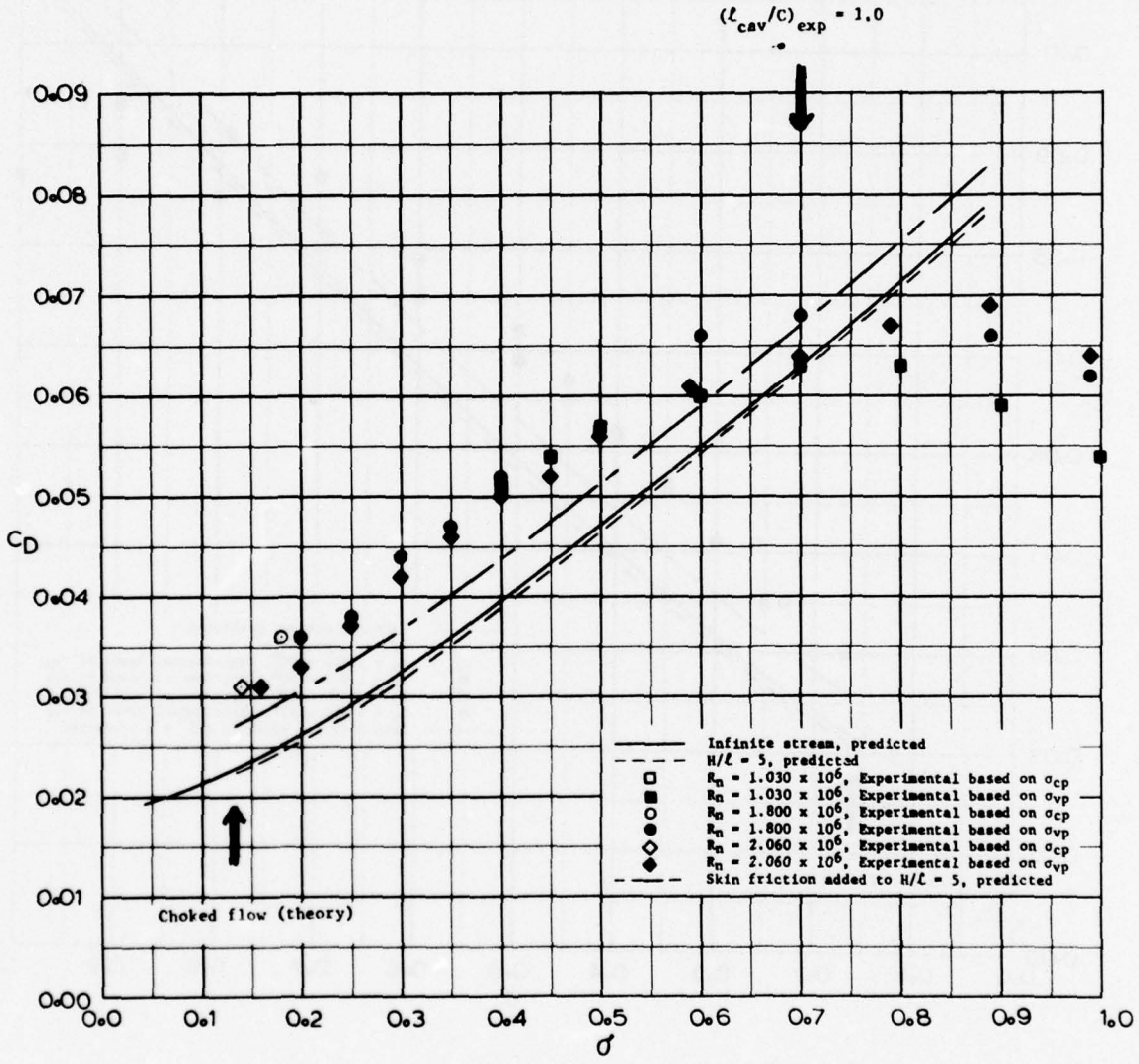

Fig. 19 - Comparison of Experimental and Predicted Drag Coefficients for 1039, $\alpha = 4.941°$

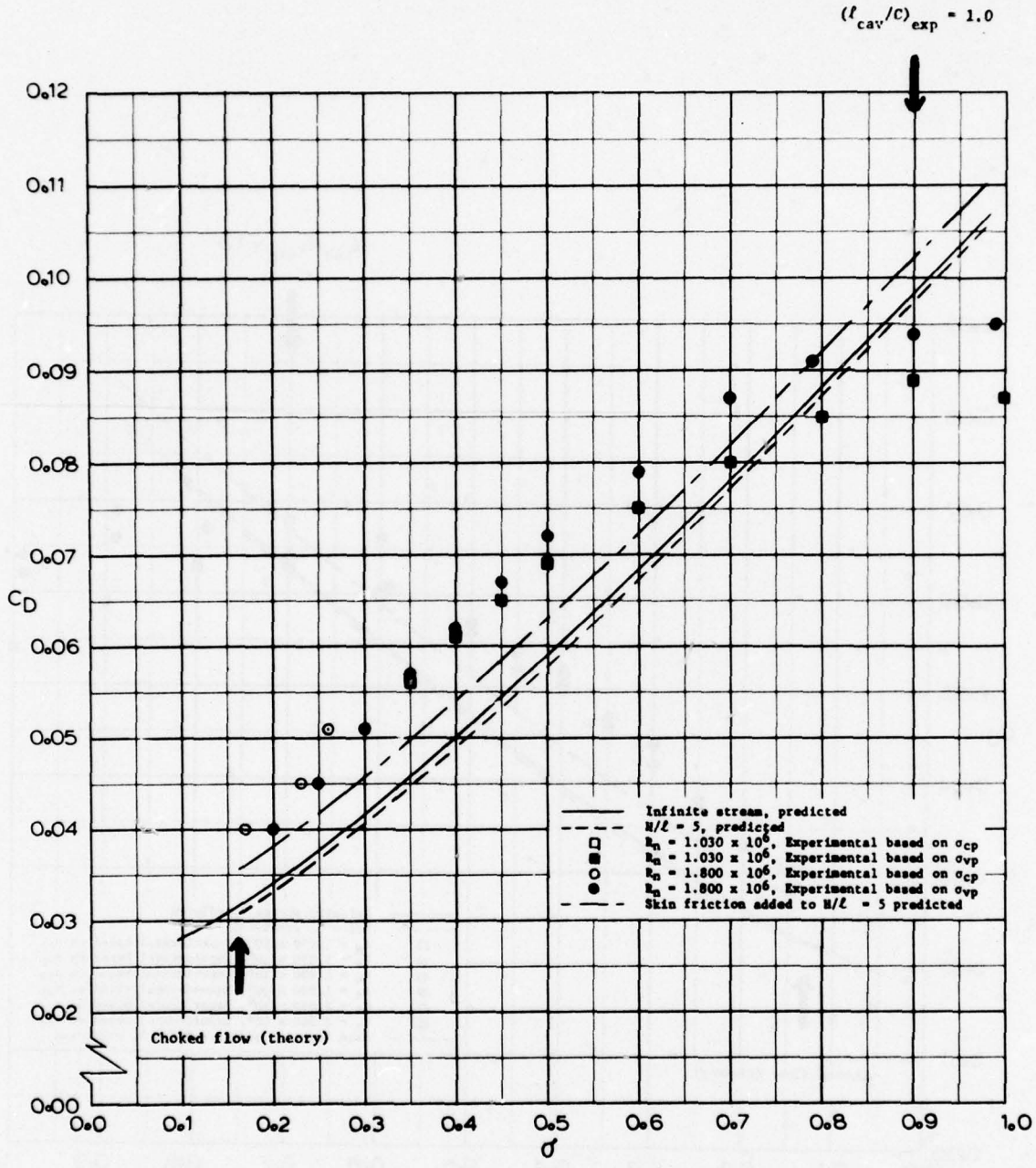

Fig. 20 - Comparison of Experimental and Predicted Drag Coefficients for 1039, $\alpha = 6.0°$

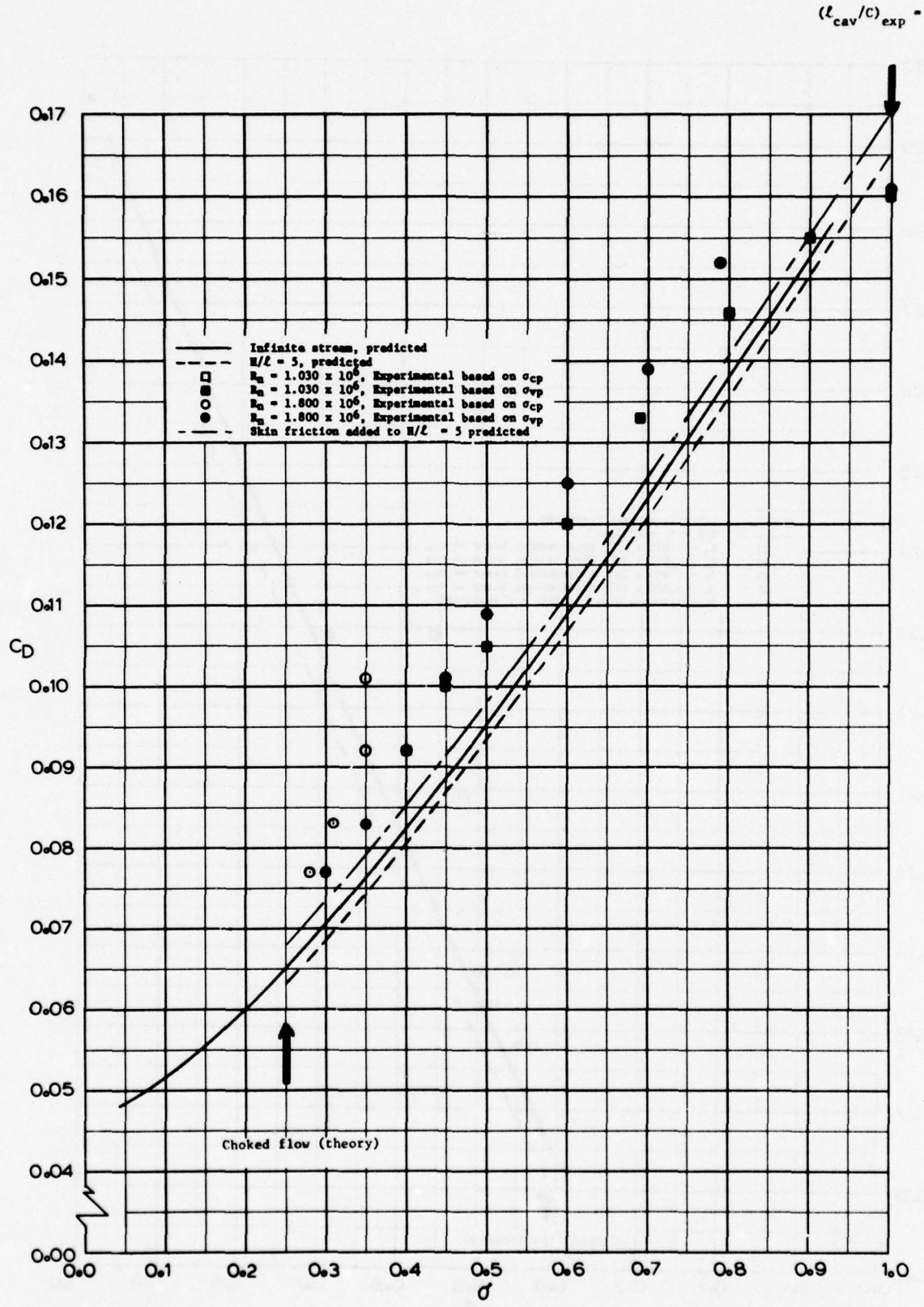

Fig. 21 - Comparison of Experimental and Predicted Drag Coefficients for 1039, α = 9.0°

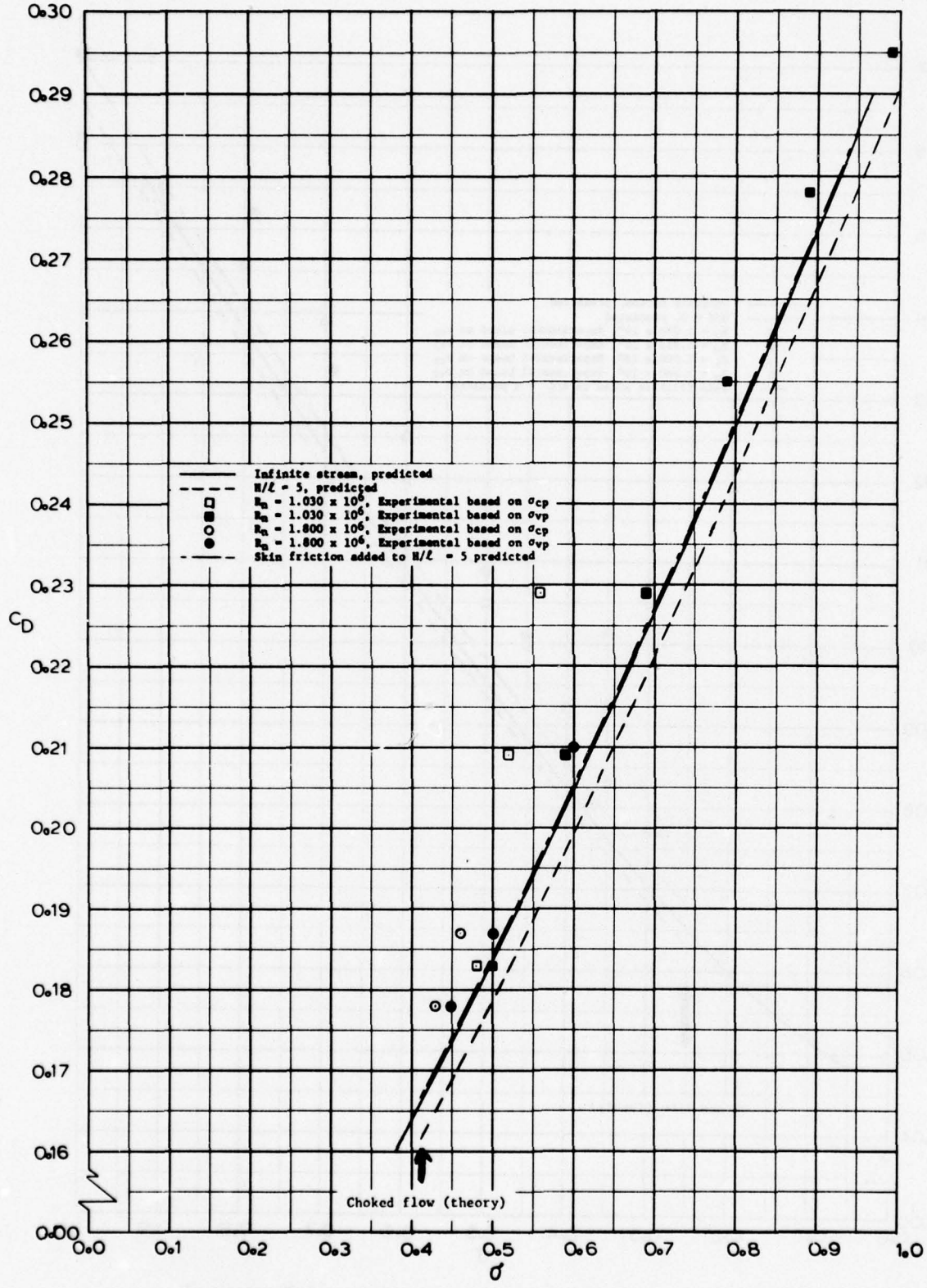

Fig. 22 - Comparison of Experimental and Predicted Drag Coefficients for 1039, α = 15.0°

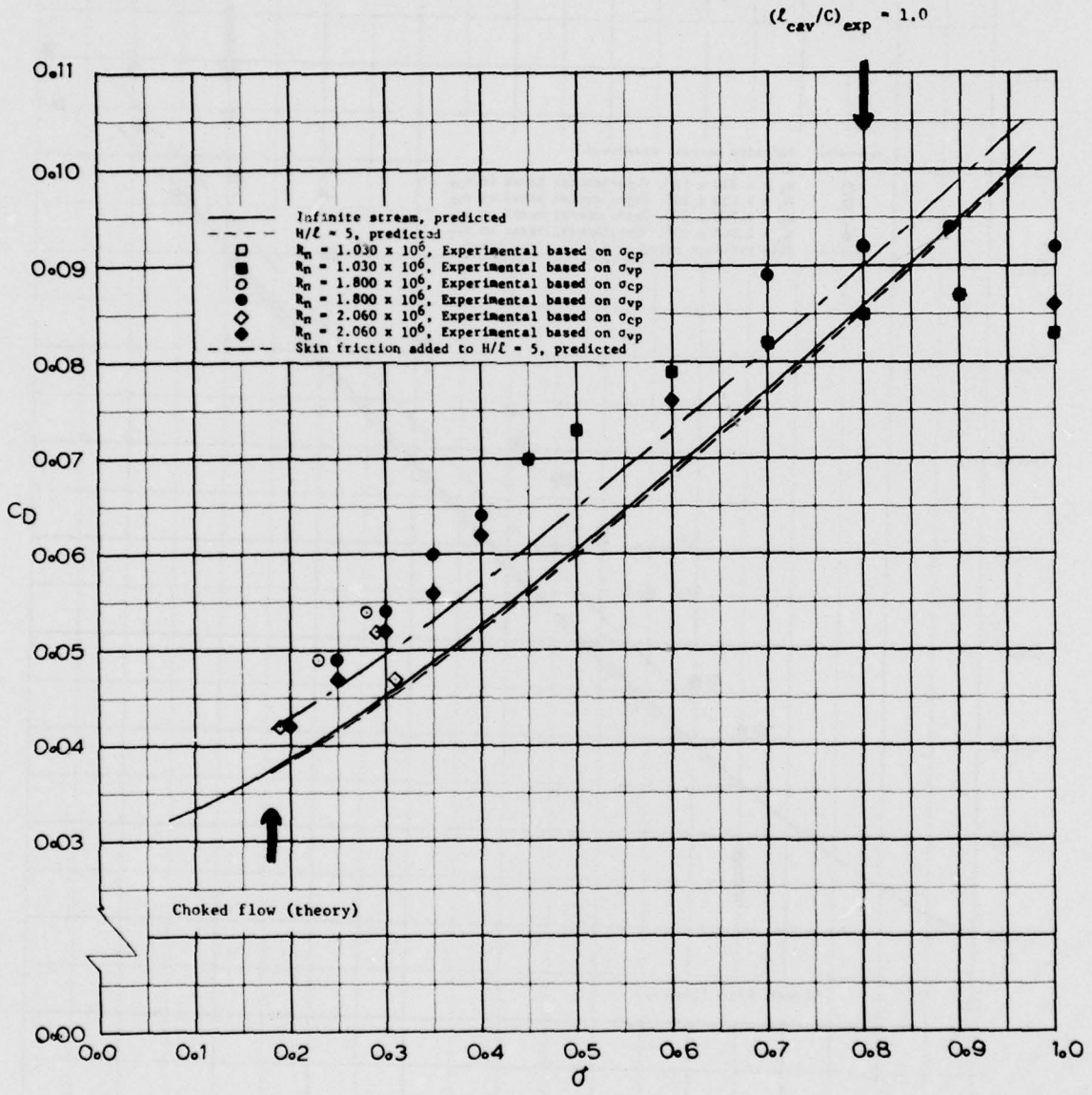

Fig. 23 - Comparison of Experimental and Predicted Drag Coefficients for 1040, α = 5.558°

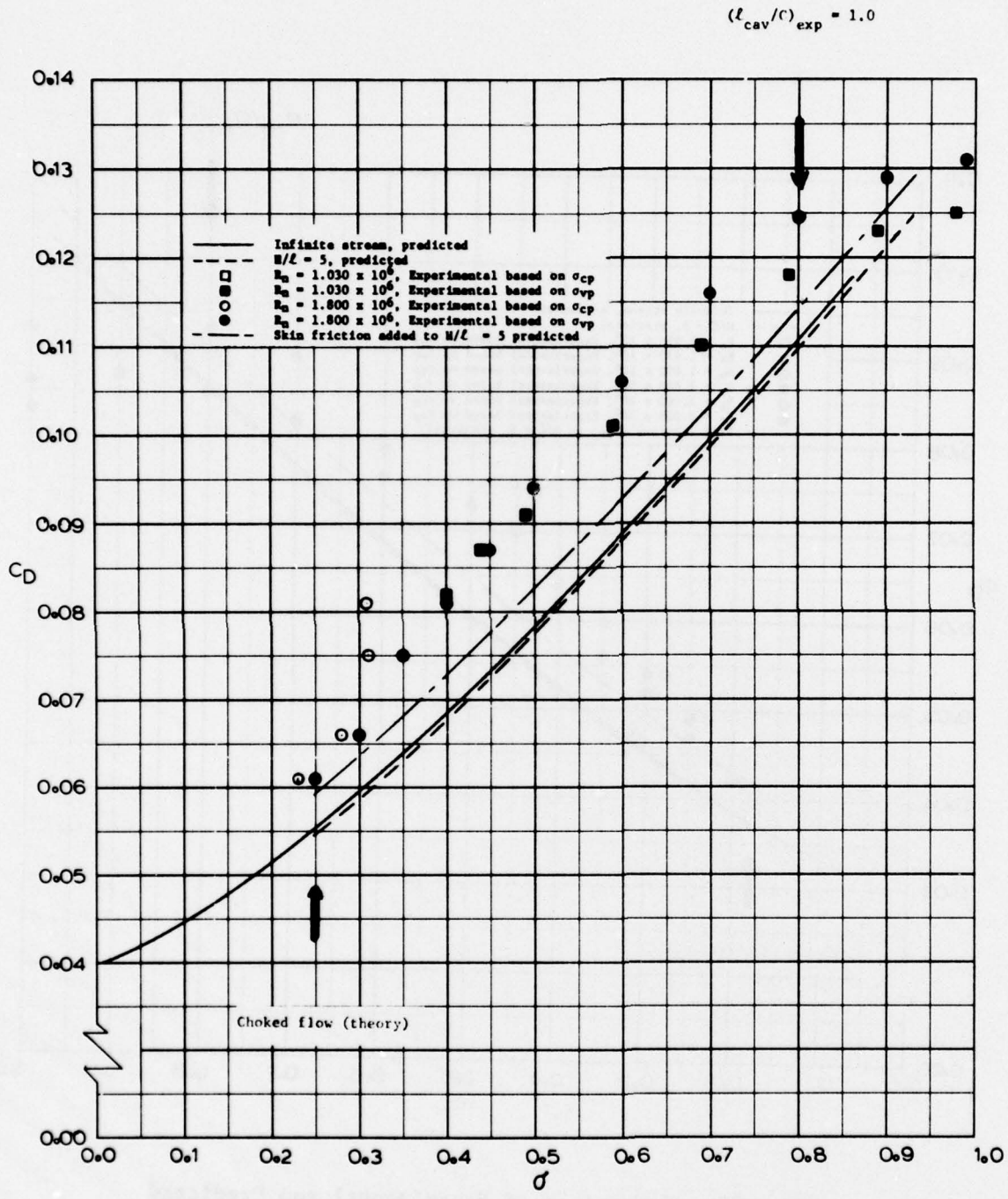

Fig. 24 - Comparison of Experimental and Predicted Drag Coefficients for 1040, $\alpha = 7.0°$

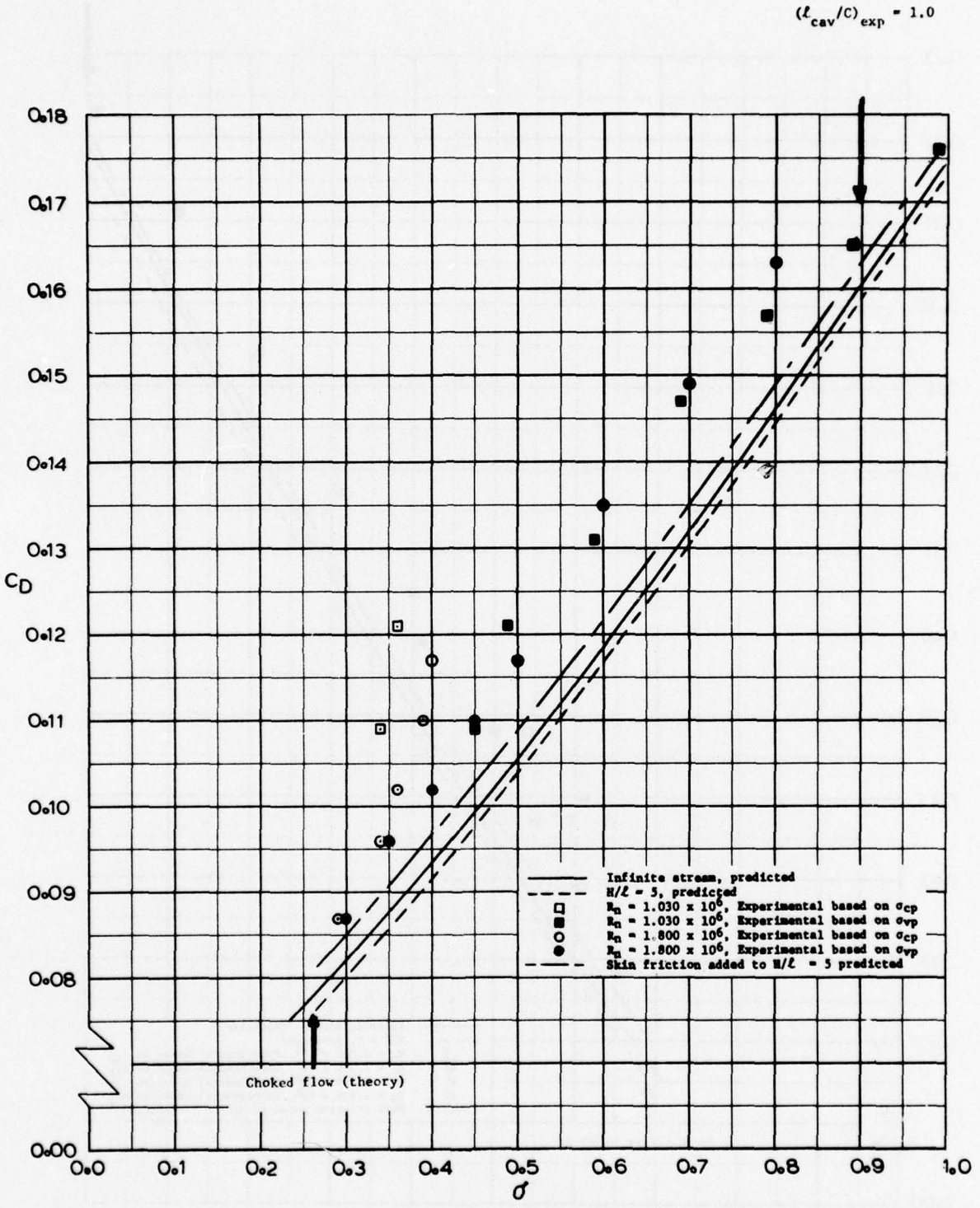

Fig. 25 - Comparison of Experimental and Predicted Drag Coefficients for 1040, α = 9.0°

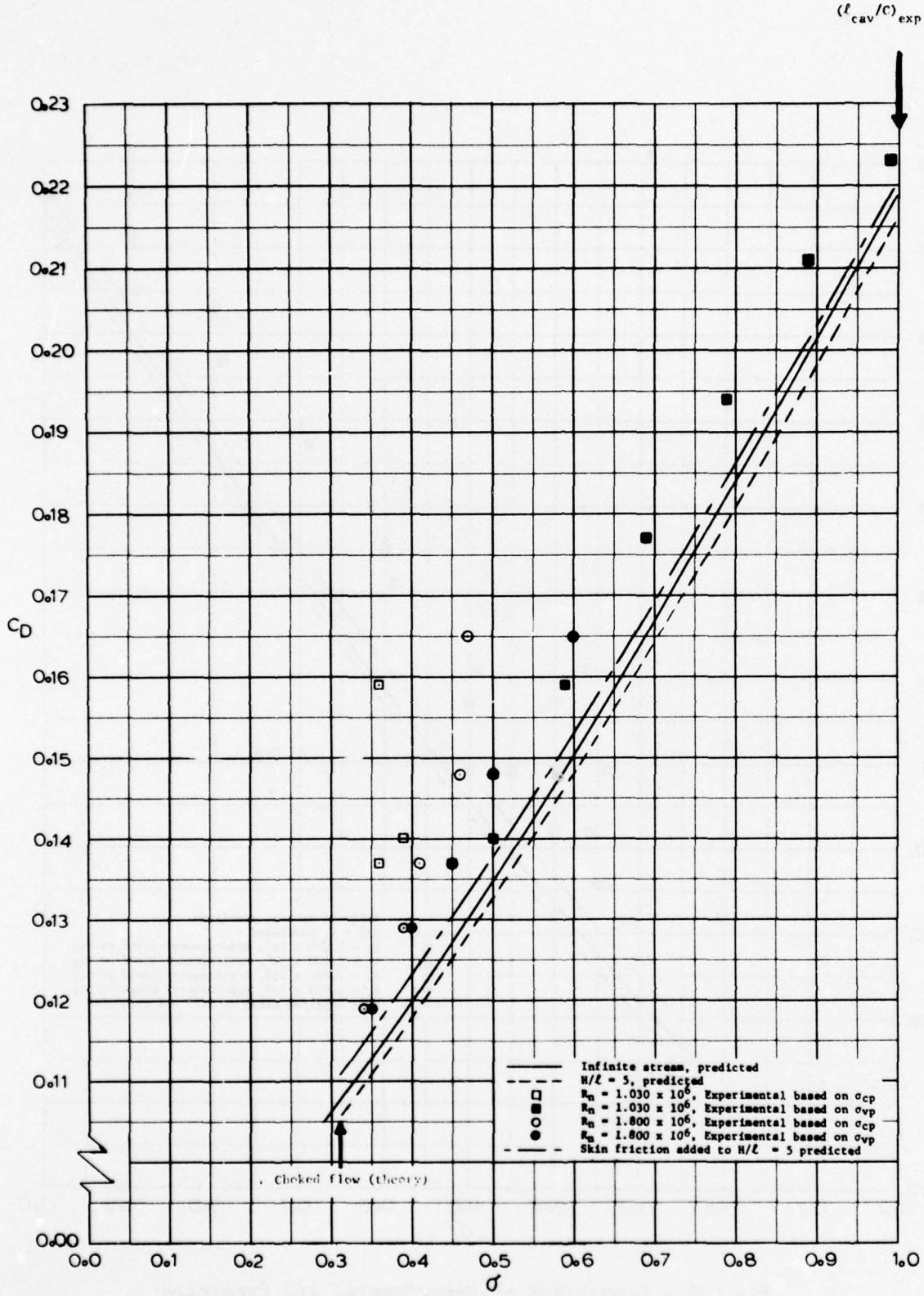

Fig. 26 - Comparison of Experimental and Predicted Drag Coefficients for 1040, $\alpha = 11.0°$

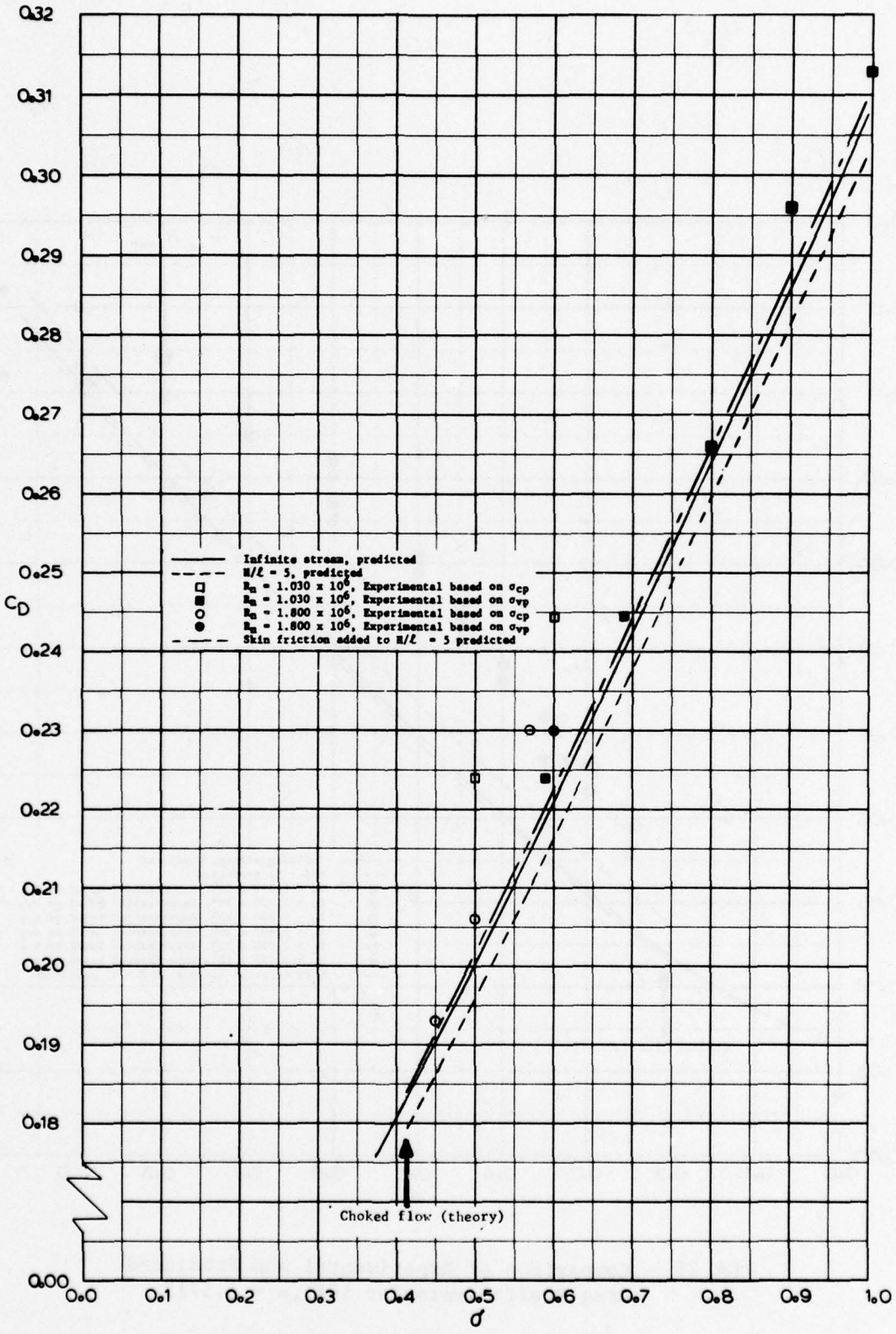

Fig. 27 - Comparison of Experimental and Predicted Drag Coefficients for 1040, α = 15.0°

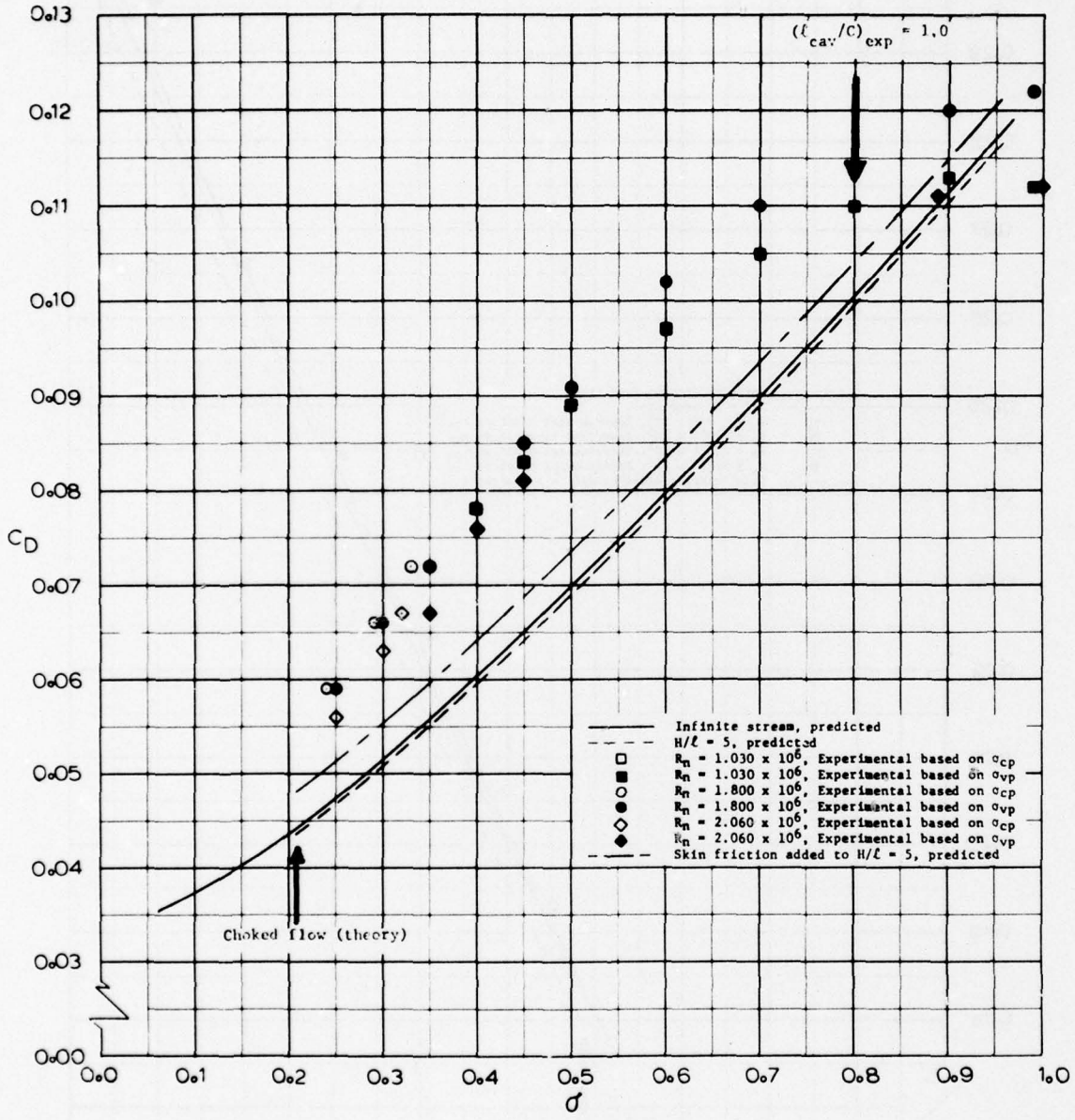

Fig. 28 - Comparison of Experimental and Predicted Drag Coefficients for 1041, $\alpha = 6.571^{\bullet}$

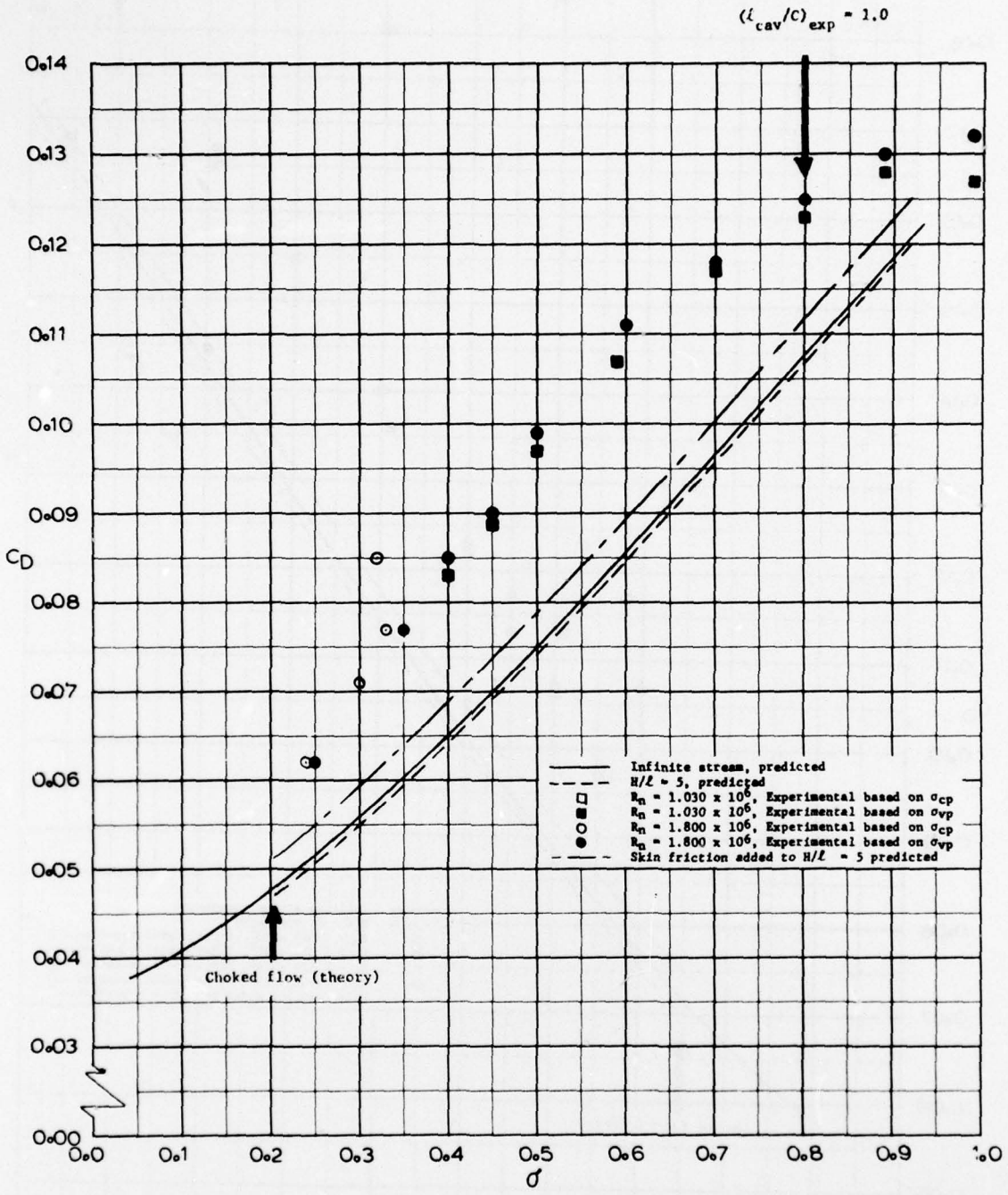

Fig. 29 - Comparison of Experimental and Predicted Drag Coefficients for 1041, $\alpha = 7.0^\bullet$

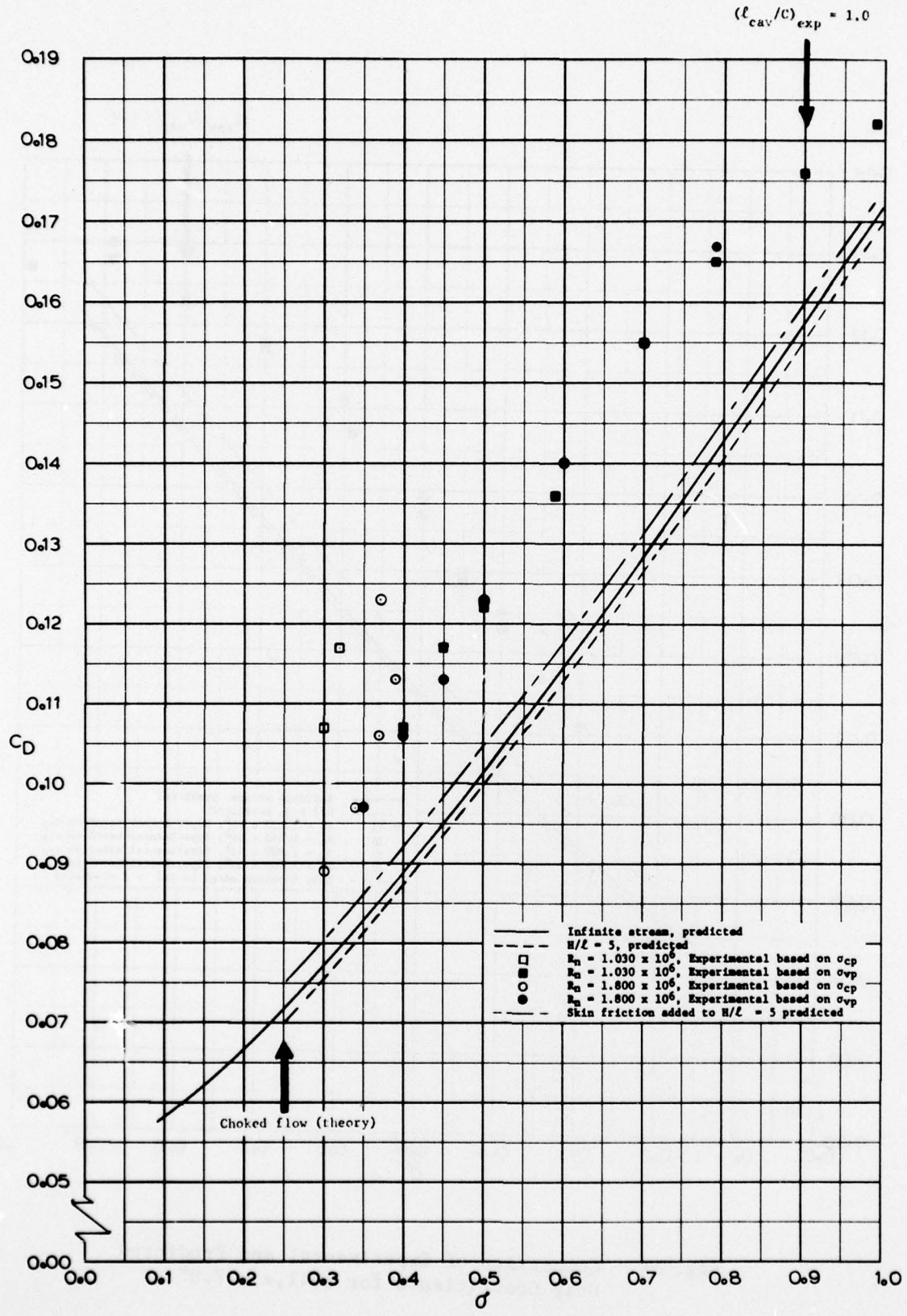

Fig. 30 - Comparison of Experimental and Predicted Drag Coefficients for 1041, α = 9.0°

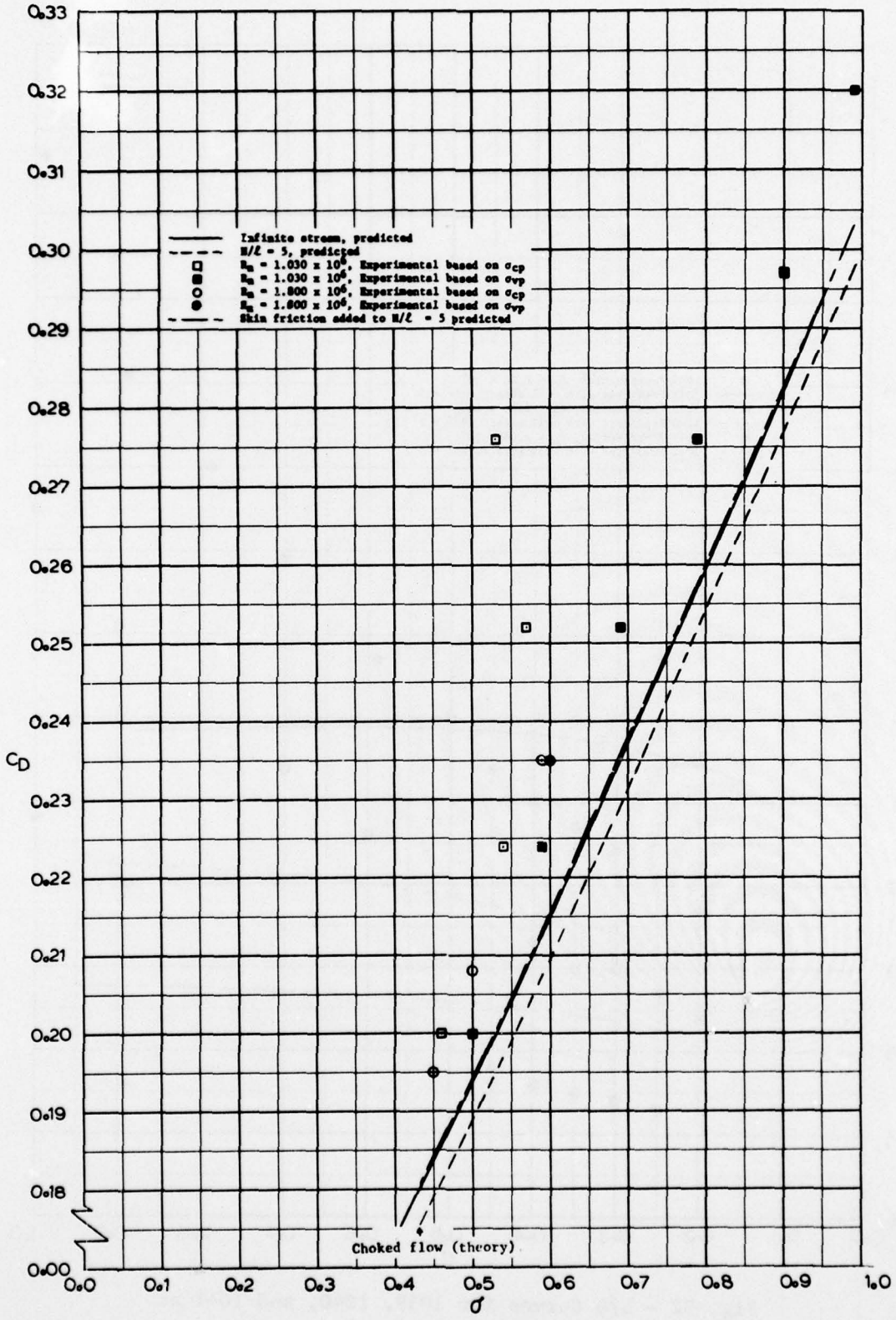

Fig. 31 - Comparison of Experimental and Predicted Drag Coefficients for 1041, α = 15.0°

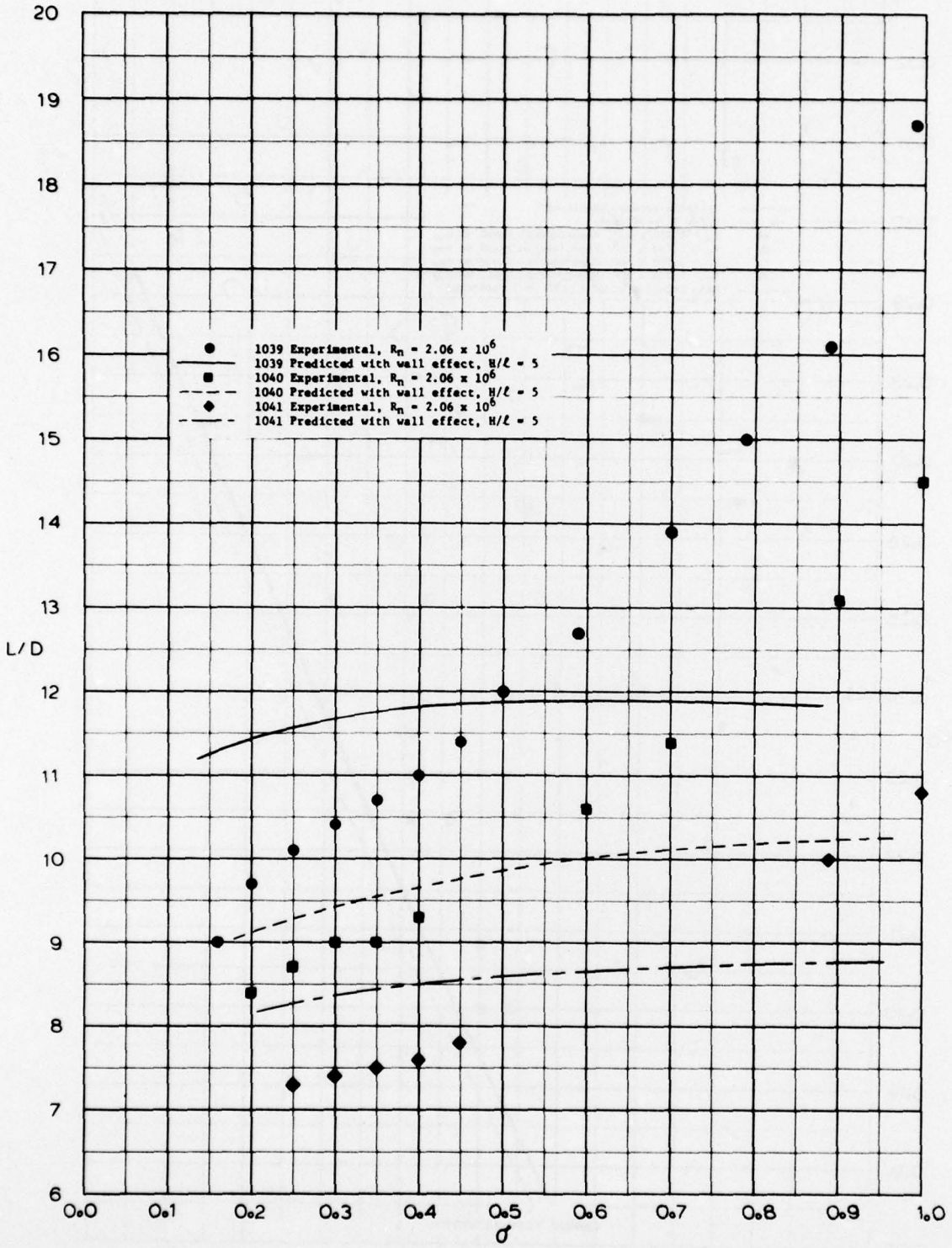

Fig. 32 - L/D Curves for 1039, 1040, and 1041 at Design Angles of Attack.

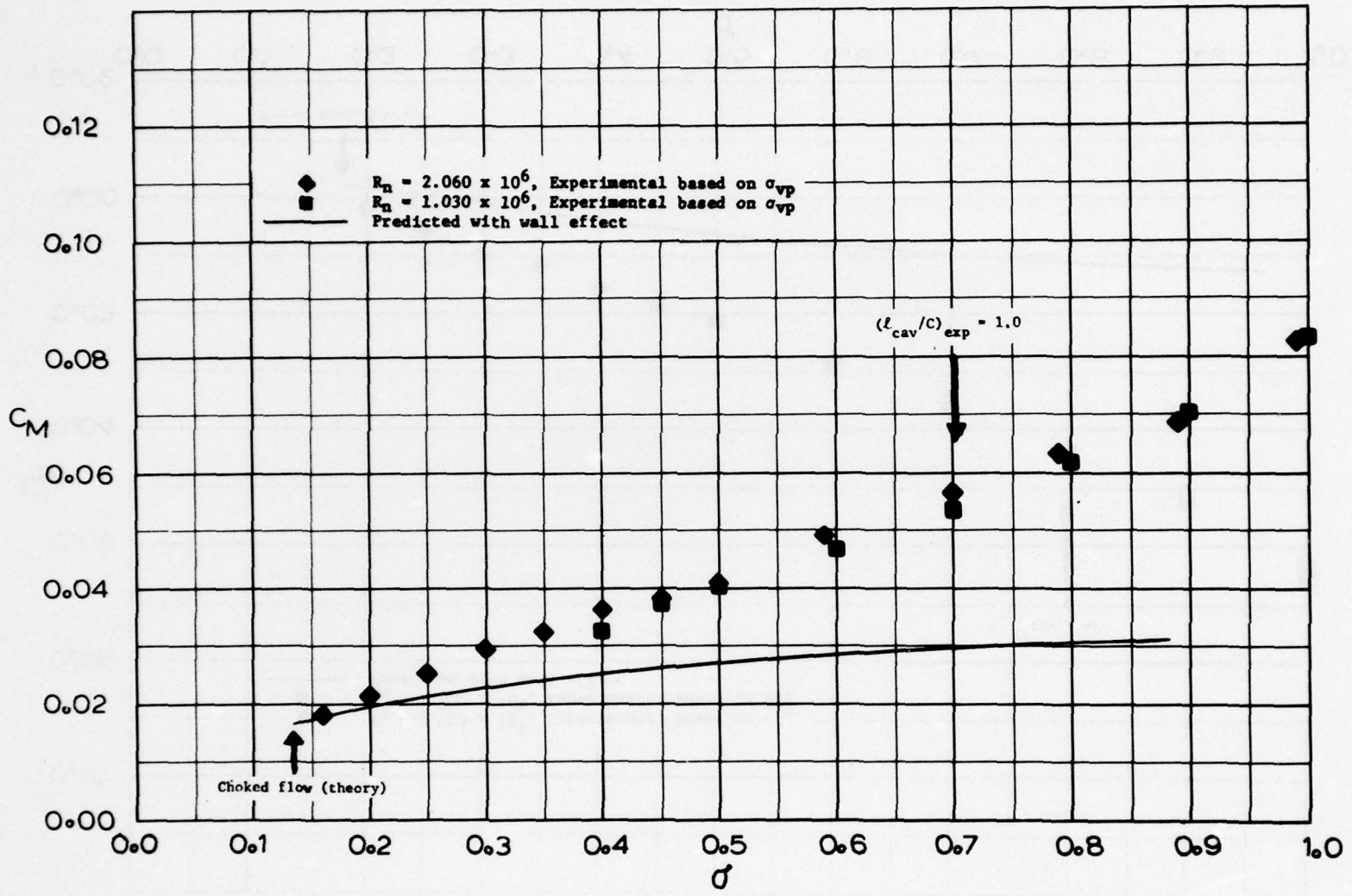

Fig. 33 - Comparison of Experimental and Predicted Moment Coefficients for 1039, α = 4.941°

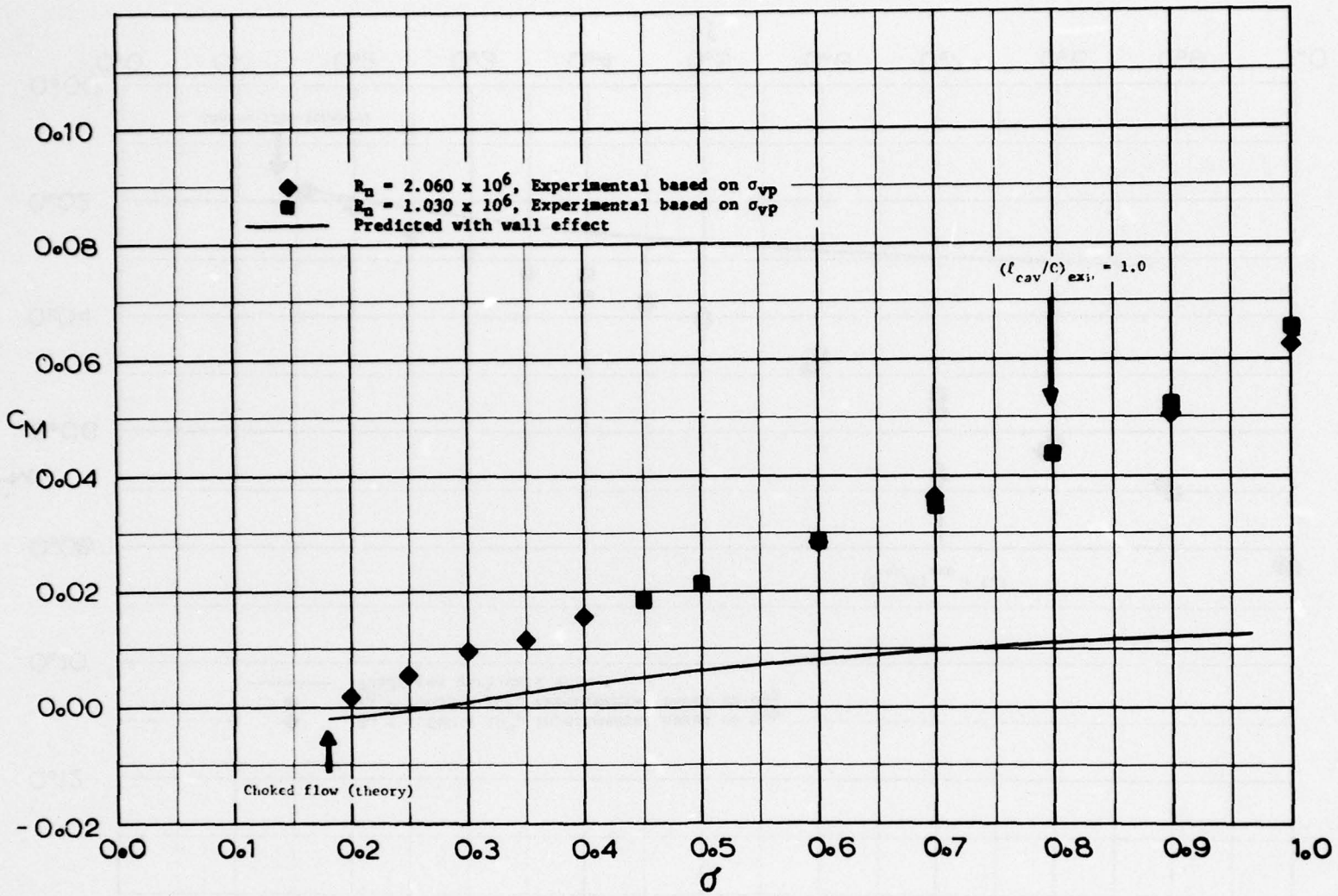

Fig. 34 - Comparison of Experimental and Predicted Moment Coefficients for 1040, α = 5.558°

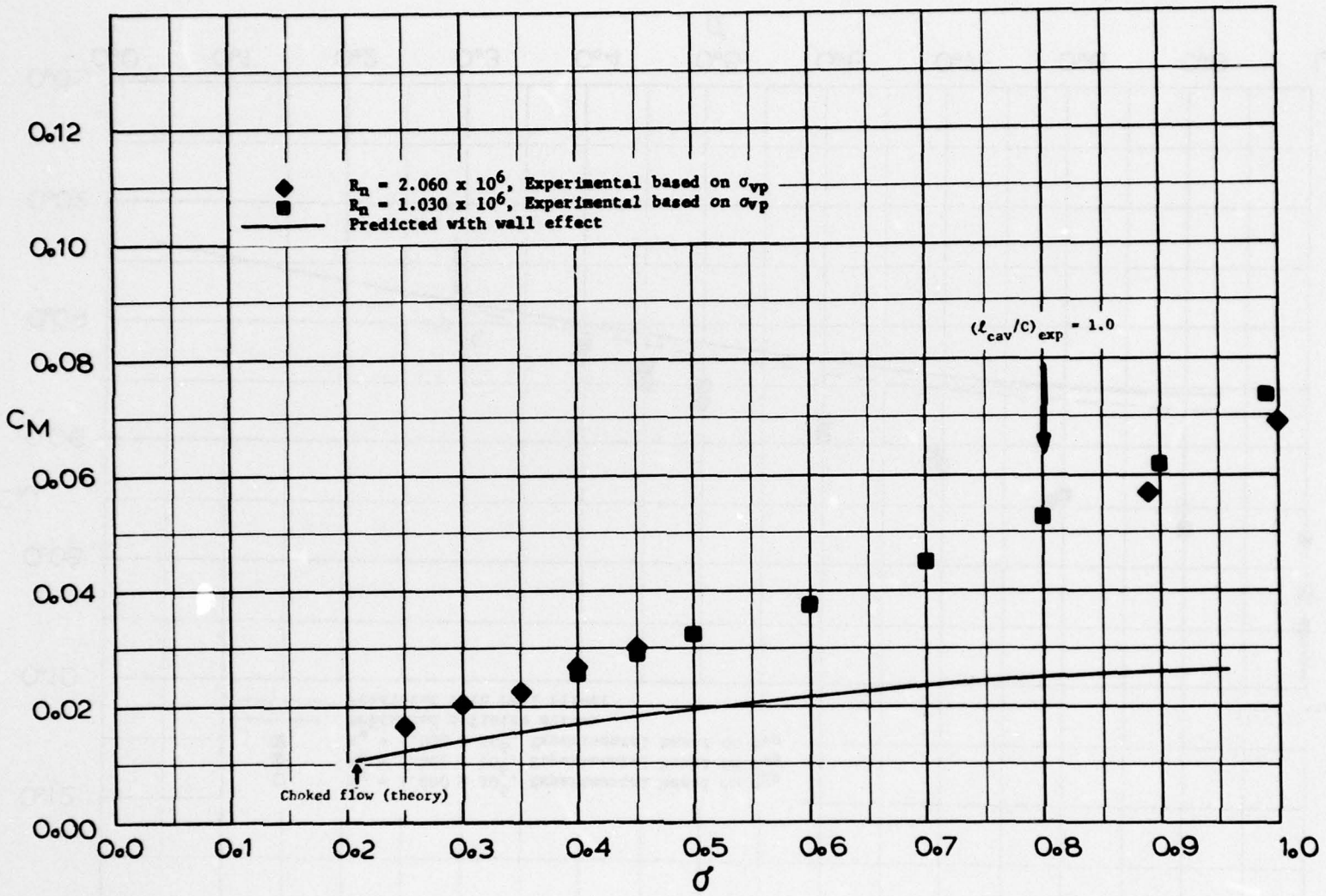

Fig. 35 - Comparison of Experimental and Predicted Moment Coefficients for 1041, $\alpha = 6.571°$

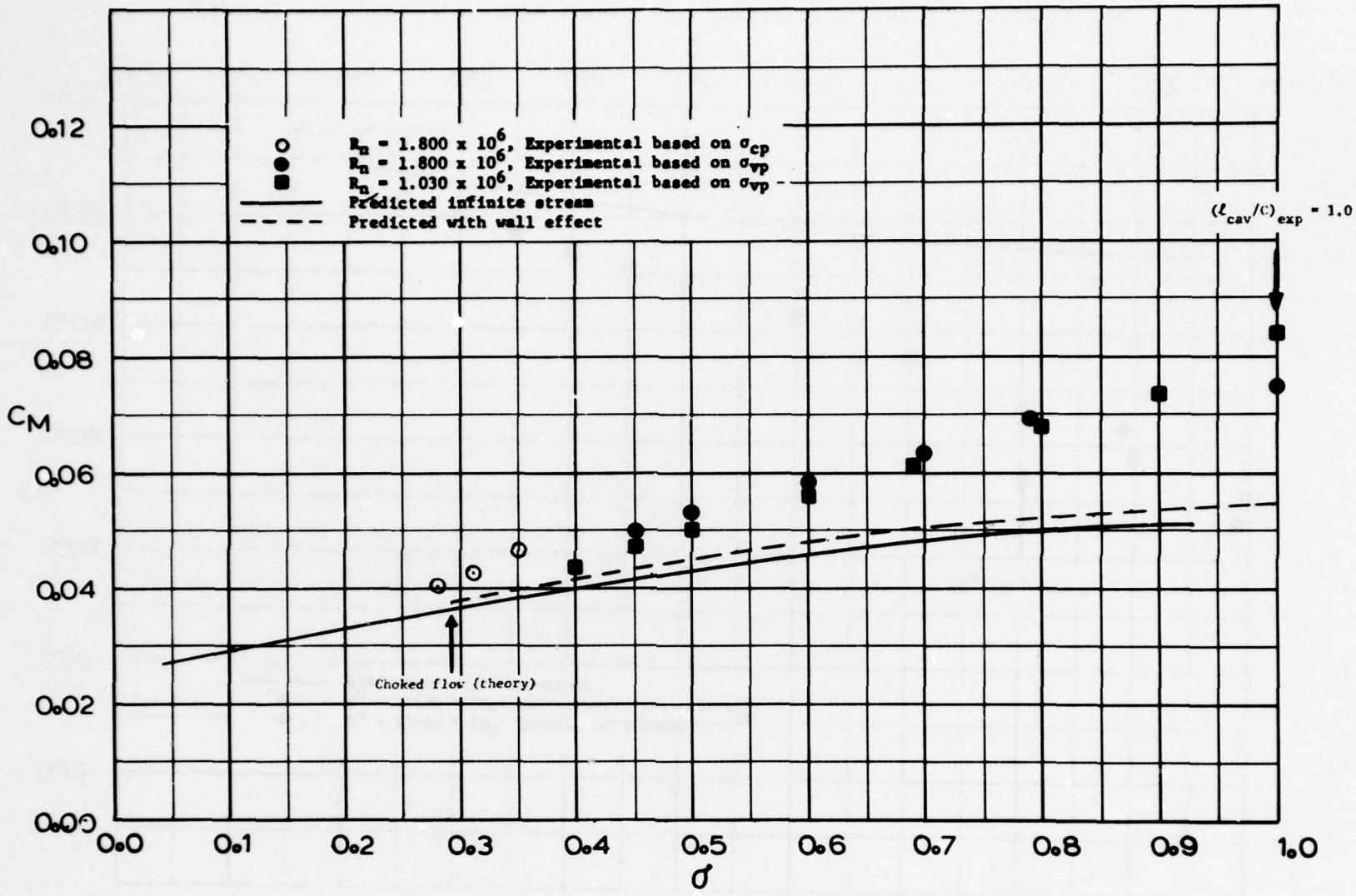

Fig. 36 - Comparison of Experimental and Predicted Moment Coefficients for 1039, α = 9.0°

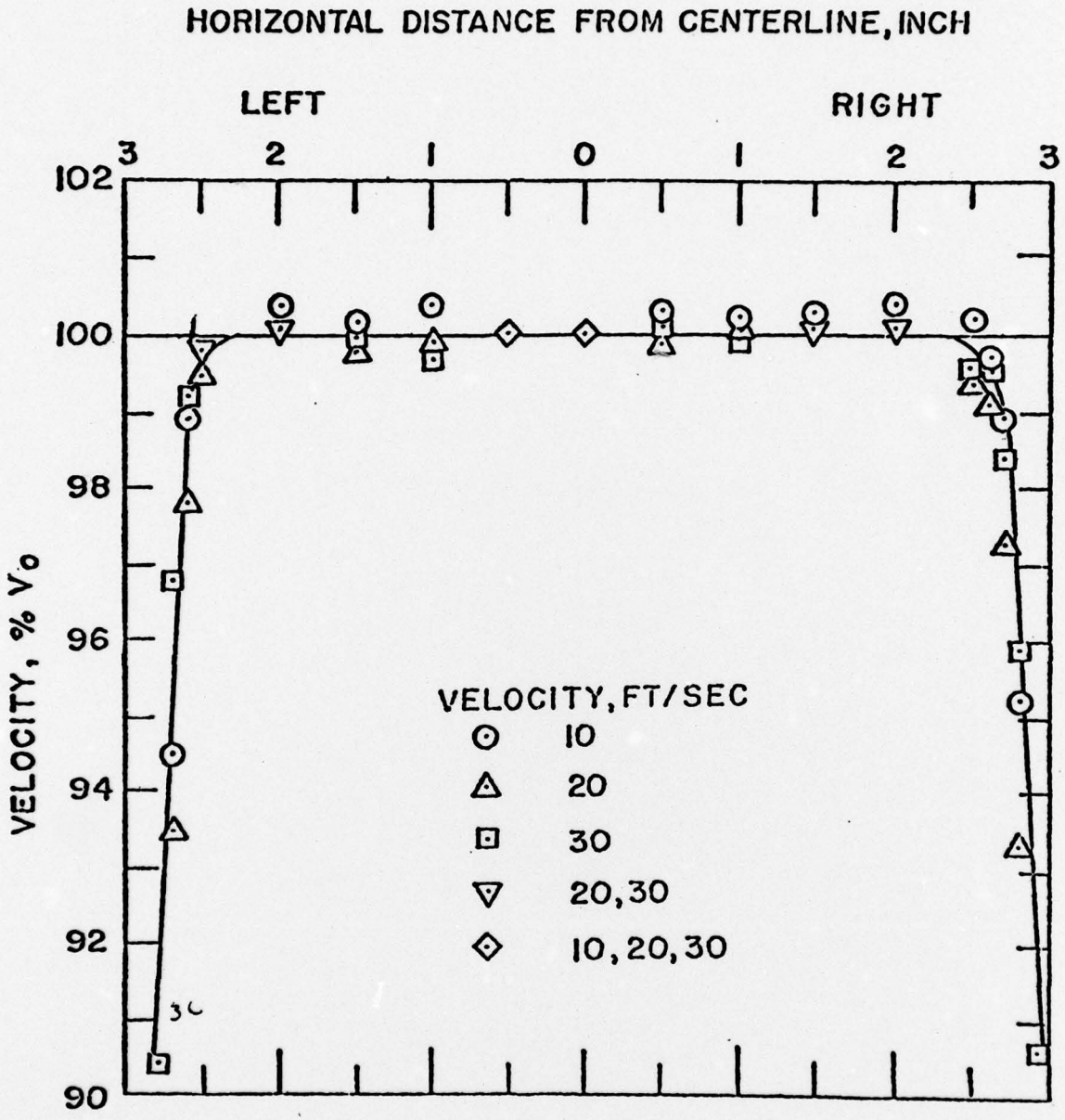

Fig. 37 - Axial Velocity Profile Along Balance Port Centerline Viewed Looking Into the Direction of Flow

This Figure is reproduced directly from Reference 6

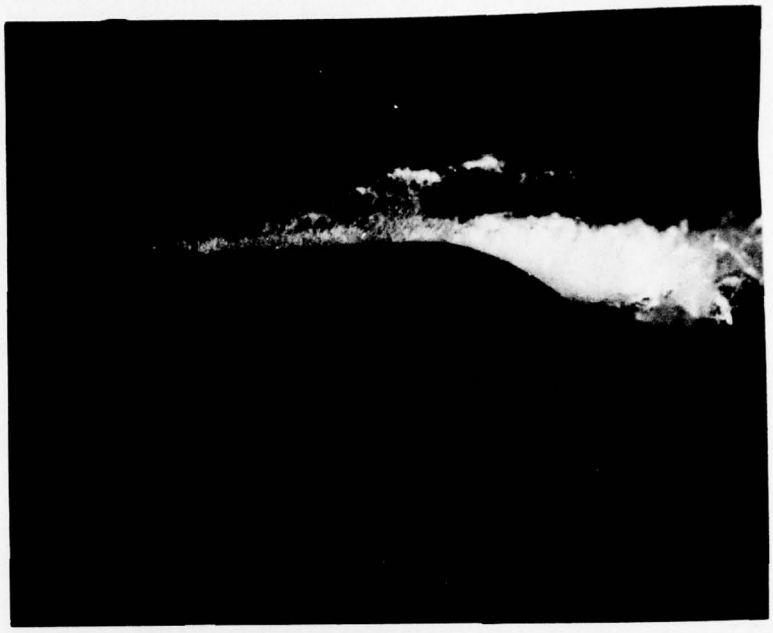

direction of flow ⟶

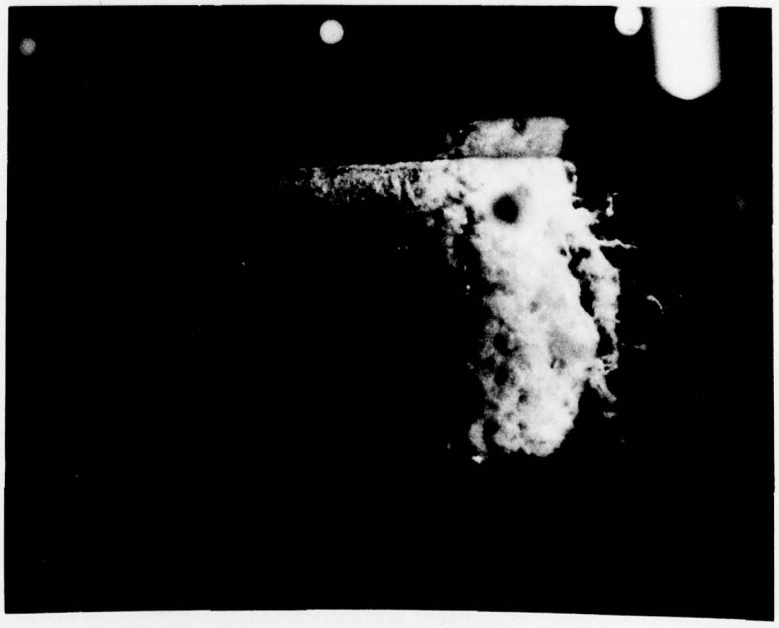

Figure 38 - Tip Vortex Occurring Between Foil Tip and Test Section Window

Figure 39 - Growth of Cavity on Foil H-1039 with Increasing Angle of Attack, at $\sigma = 0.50$

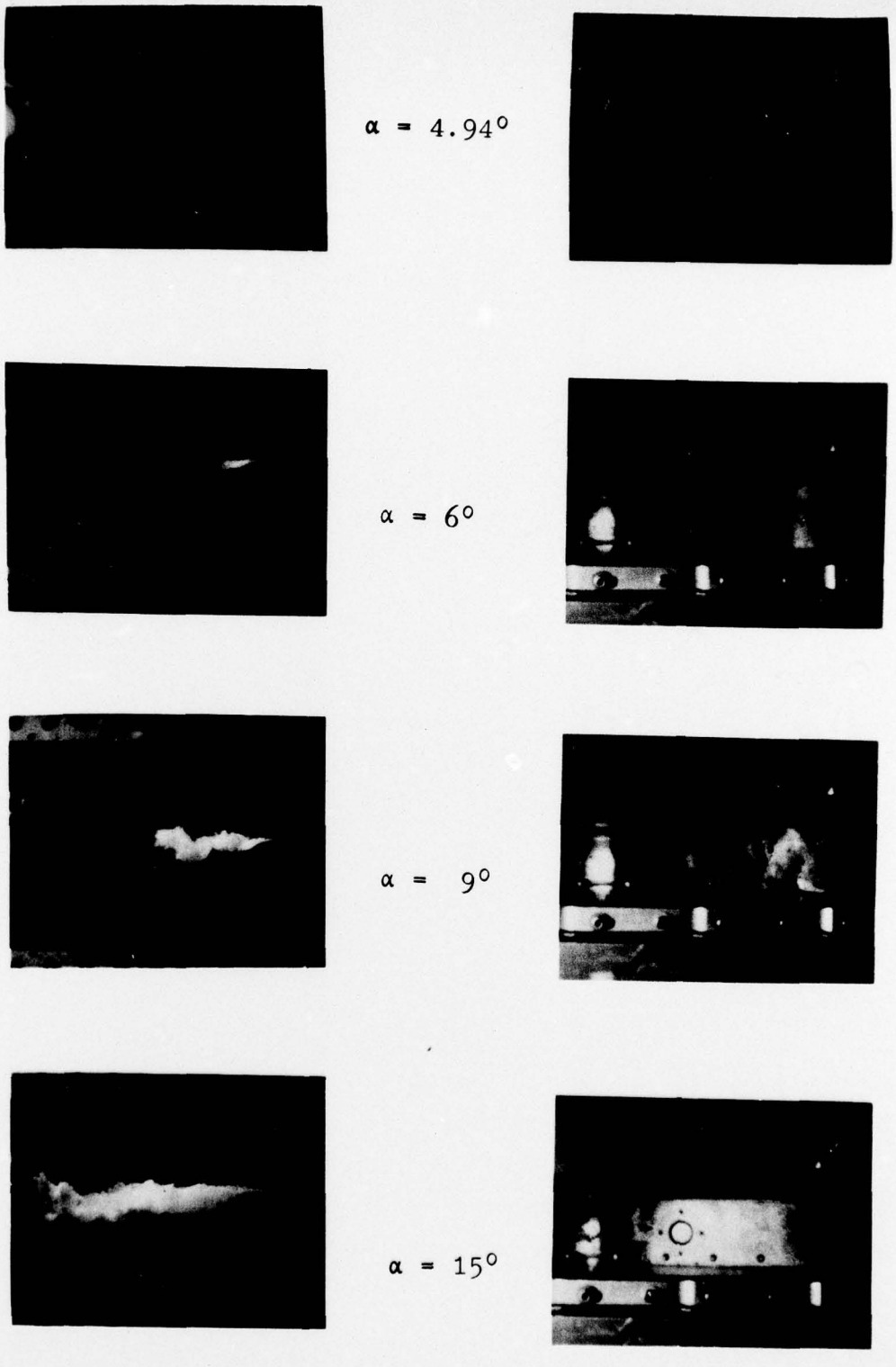

Figure 40 - Growth of Cavity on Foil H-1039 with Decreasing Cavitation Number, at α 4.94°

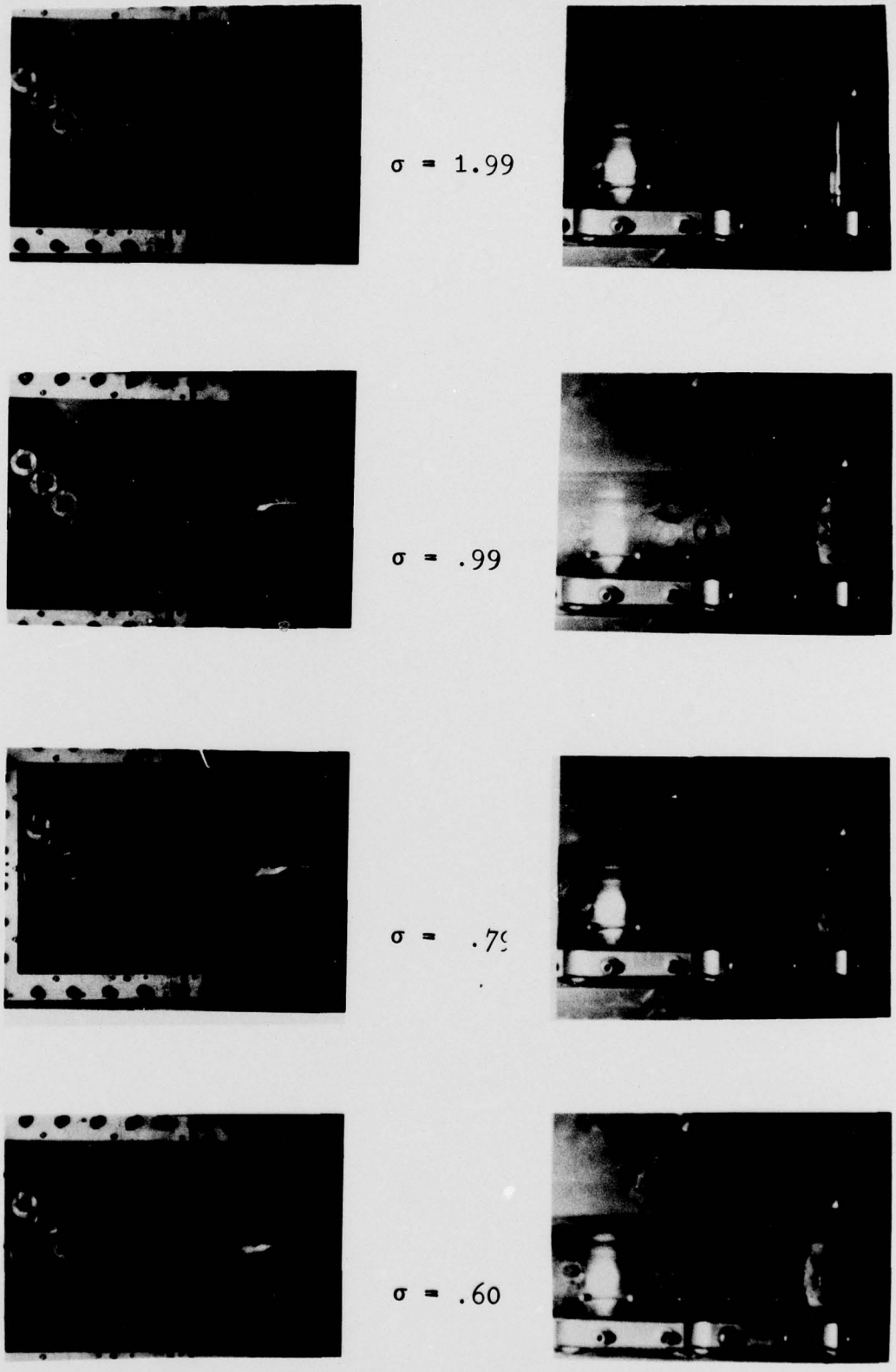

Figure 40 - Continued

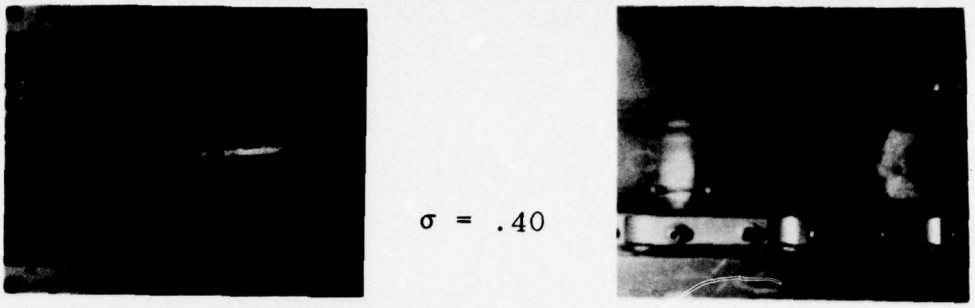

σ = .40

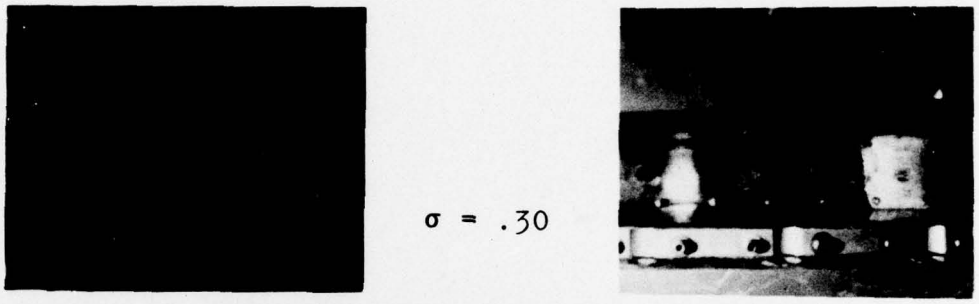

σ = .30

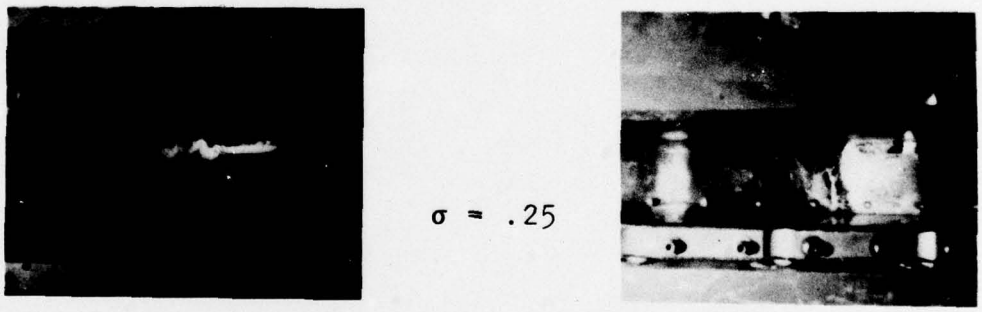

σ = .25

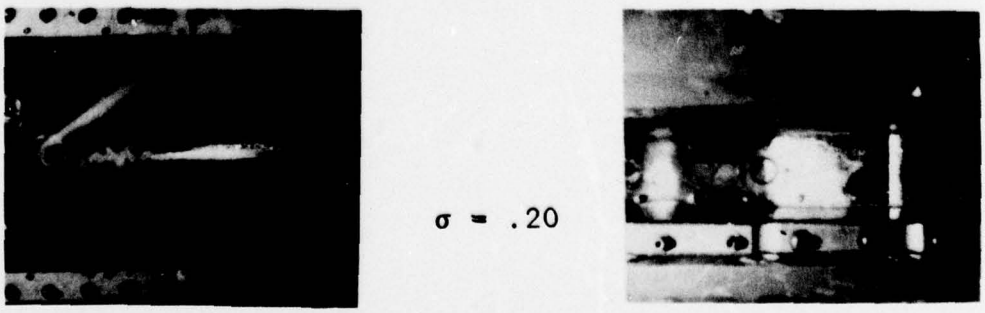

σ = .20

← direction of flow

DTNSRDC ISSUES THREE TYPES OF REPORTS

(1) DTNSRDC REPORTS, A FORMAL SERIES PUBLISHING INFORMATION OF PERMANENT TECHNICAL VALUE, DESIGNATED BY A SERIAL REPORT NUMBER.

(2) DEPARTMENTAL REPORTS, A SEMIFORMAL SERIES, RECORDING INFORMATION OF A PRELIMINARY OR TEMPORARY NATURE, OR OF LIMITED INTEREST OR SIGNIFICANCE, CARRYING A DEPARTMENTAL ALPHANUMERIC IDENTIFICATION.

(3) TECHNICAL MEMORANDA, AN INFORMAL SERIES, USUALLY INTERNAL WORKING PAPERS OR DIRECT REPORTS TO SPONSORS, NUMBERED AS TM SERIES REPORTS; NOT FOR GENERAL DISTRIBUTION.